NPS ARCHIVE
1967
STROHSAHL, G.

CONSTRUCTION AND CALIBRATION OF A MASS SPECTROMETER FOR THE ANALYSIS OF LIGHT IONS

GEORGE HENRY STROHSAHL

CONSTRUCTION AND CALIBRATION OF A MASS SPECTROMETER FOR THE ANALYSIS OF LIGHT IONS

by

George Henry Strohsahl, Jr.
Lieutenant, United States Navy
B.S., Naval Academy, 1959

[redacted]

Submitted in partial fulfillment of the
requirements for the degree of
MASTER OF SCIENCE IN PHYSICS
from the
NAVAL POSTGRADUATE SCHOOL
December 1967

67
TROSAHL, G.

ABSTRACT

A magnetic mass spectrometer employing a 45° bending angle was constructed and calibrated as part of an experimental apparatus to study ion-molecule rearrangement collisions. It has a resolution ($m/\Delta m$) of about 40 with beam transmission in excess of 90%, and it will mass analyze charged particles up to mass number 40 with energies up to 1 KEV. The spectrometer, using a magnet current of 8 amps, has a maximum field strength of about 4 Kilogauss confined between 40° wedge sector shaped pole pieces with a 3/4" gap width. Magnet current curves are given for mass analysis of ions through mass number 7 as a function of kinetic energy. A plasma source using electron-impact ionization was used to generate the ion beams of mass 1 to 4 while a thermal β-eucryptite source was used to produce Li^+ beams of mass 6 and 7. Measurements of the energy spread of the ion beams indicate a typical value of $\Delta E/E = 4\%$ for the gas source and 1% for the thermal emitter. Subject to a specified degaussing procedure the beam energy can be written as a function of magnet current in the form $E = C_3 I^2 + C_2 I + C_1$. Tables giving both experimentally and theoretically determined values of the coefficients C_3, C_2 and C_1 as a function of ion mass are presented.

TABLE OF CONTENTS

Page

List of Tables 5

List of Illustrations 7

Acknowledgements 8

I Introduction 9

II Experimental Apparatus 11

  A Mass Spectrometer 11

  B Vacuum System 21

  C Gas Ion Source 23

  D Lithium Ion Source 28

  E Beam Detector 33

  F Energy Analyzer 35

III Experimental Procedures 41

  A Magnetic Field Measurements 41

  B Mass Calibration 46

IV Analysis of Results 54

Bibliography 58

Appendix I 59

Appendix II 62

Initial Distribution List 65

LIST OF TABLES

Page

Table I Coefficients of the Second Order Polynomials Describing the Experimentally Determined Mass Spectrometer Operation Curves. 53

Table II Coefficients of the Second Order Polynomials Describing the Theoretically Determined Mass Spectrometer Operating Curves. 64

LIST OF ILLUSTRATIONS

Figure Number	Title	Page
1.	Cross-sectional View of Mass Spectrometer	16
2.	Side View of Mass Spectrometer	17
3.	Mass Spectrometer and Scattering Apparatus	18
4.	Rear View of Mass Spectrometer	19
5.	Schematic of Magnet Control Circuit	20
6.	Cross-sectional View of Gas Ion Source	27
7.	Lithium Source: Emitter Temperature vs Filament Power Curve	30
8.	Cross-sectional View of Lithium Source	31
9.	External View of Gas and Lithium Sources	32
10.	Schematic of Electrostatic Energy Analyzer	37
11.	Beam Detector and Energy Analyzer In Position	38
12.	Schematic of Calibrating Apparatus	39
13.	External View of Calibrating Apparatus	40
14.	Spectrometer Magnetization Curve	44
15.	Spectrometer Magnetic Fringing Field	45
16.	Typical Spectrometer Mass Trace at 300 eV	50
17.	Retarding Field Curve at 311 eV for Li^7	51
18.	Spectrometer Operation Curves	52

ACKNOWLEDGEMENTS

The thoughtful assistance and encouragement of Dr. Otto Heinz, Chairman, Physics Department, Naval Postgraduate School, as advisor for this project is gratefully acknowledged. Additionally the advice of Dr. Charles Cook and Dr. William Aberth of the Stanford Research Institute is appreciated.

Much preliminary work and continuing experimental investigation of many aspects of this project was done by LT Thomas O. Bush, USN, a PhD candidate at the Postgraduate School and his assistance was of great benefit.

Finally, none of this could have been accomplished without the tireless and extremely competant efforts of Mr. Thomas Maris of the technical staff of the School.

I INTRODUCTION

The design, construction, and calibration of a small mass spectrometer as described in this paper was undertaken primarily in support of an experimental atomic scattering project presently being conducted at the Naval Postgraduate School. This project proposes to measure the cross section for the capture of a light ion or atom from a gaseous target by an ionic projectile. The purpose of these measurements is to obtain experimental data in support of a classical theory developed by Bates, Cook, and Smith[1] which predicts such cross sections.

The expected cross sections are of the order of $10^{-20} cm^2$ or less and thus too small to measure by normal differential scattering techniques. Therefore an apparatus based on the principle of a thin lens beta-ray spectrometer was designed which increases the solid angle by a factor of several hundred over that obtainable by conventional differential scattering techniques. The particular reaction to be experimentally investigated is the capture of a hydrogen atom by a fast proton in an ion-molecule rearrangement collision with methane. This can be written as:

$$H^+ + HCH_3 \longrightarrow H^+ H + CH_3$$

The classical theory of Bates, et.al., is valid for a projectile energy range of 25 to 800 eV, and a scattering angle in the vicinity of 45 degrees.

To provide protons of this energy range, an electron impact type ion source was constructed and its properties investigated. It was found that the resultant ion beam contained the species H^+, H_2^+, and H_3^+ in varying ratios depending on the exact operating conditions within the ion source. Feist[2] has shown that the cross section for elastic scattering of H_2^+ from atomic carbon is comparable to the rearrangement cross section to be measured. Since the resulting H_2^+ ions have the same momentum in both cases it is necessary to remove any H_2^+ ions present in the incident beam. Additionally the relatively low proton intensity from the ion source makes it necessary to achieve a high transmission factor in the separation process.

The goal of this project was therefore to design and construct a mass spectrometer which combines maximum beam transmission with sufficient resolution to separate ions with mass numbers up to 40 and energies up to about 1 keV.

II EXPERIMENTAL APPARATUS

A. Mass Spectrometer

The design specifications for both physical dimensions and operating capabilities of the mass spectrometer were based primarily on the requirements of the previously described scattering experiment. The resulting hardware had to be dimensionally compatable with the main body of the scattering apparatus, the ion sources, and the vacuum pumping system.

The first general decision was the determination of the bending angle to be employed. Here a compromise was necessary between the requirements of resolution and transmission. Prior experience with a mass spectrometer on loan from the Stanford Research Institute, which used a 60° bending angle showed that good resolution could be obtained with this angle. However the transmission loses due to beam defocusing which are approximately inversely proportional to the bending angle for angles less than about 90°, would be too great. Therefore the angle of 45° was selected to offer improved transmission while, hopefully, not degrading the resolution appreciably. This choice of angle has proven to be quite adequate.

The next decision involved the construction of the bending magnet. The requirements of being able to separate the three ion species of molecular hydrogen with energies of less than 100 eV and still be capable of analyzing masses up to about mass number 40 with energies of several kilovolts established a variable field strenth from 50 gauss up to 5000 gauss. Again, the experience with the SRI mass spectrometer showed that the magnet it employed was capable of this range with the only undesirable characteristic being a very low coil current requirement with attendant regulation difficulties for the 50 to 500 gauss field range. Since the general size parameters of the proposed spectrometer were known to be of the order of the SRI mass spectrometer, it was decided to use the plans for the SRI magnet with the change that the two current coils of the magnet would be split making essentially four separate coils. The field range could then be selected by changing the number of coils used and a reasonable magnet current could be used. The plans for the magnet were obtained from SRI and used by the Pacific Electric Company of Oakland, California to manufacture the magnet.

Another design decision involved the location of the magnet poles in relation to the spectrometer body. The question of whether the pole pieces should be internal or external to the spectrometer body was resolved in favor of the external configuration in order to afford the following advantages to the overall system:

(1) Enhanced vacuum integrity by reducing the number of joints and seals in the system.

(2) Increased flexibility of configuration by allowing the changing of pole piece orientation for beam focusing or substitution of different geometry pieces while the system remains under vacuum.

(3) Elimination of soft iron components from within the system enhancing the system cleanliness.

A few dimensional decisions were arbitrarily made during the design process for which, perhaps, some justification should be given. The pumping port (see Fig. 1) was designed as six inches to take best advantage of the six-inch manifold on the vacuum pumping system and provide optimum pumping speed. The space between the internal pole faces was selected as 3/4 inch as a compromise between the desire to keep the gap width small and yet permit unhindered passage of the entire ion beam which was known to have a diameter of approximately one centimeter at the distance from the source to be used. The pumping port was placed behind the pole pieces, with respect to the ion flow direction, to keep the total distance from ion source to scattering chamber as short as possible to enhance transmission. For the same reason, the ion source spool was made only as long as necessary to accomodate the gas ion source, complete with lens and deflector shims. A lucite window was provided at the rear of the spectrometer concentric to the beam axis to allow visual alignment of the entire system and viewing during operation. The position of the pole pieces was chosen so that the particle trajectories would pass through the pole's center. The pole pieces were designed with a 40^o wedge sector giving the incident beam a 5^o from normal angle of incidence at the entrance pole face. The rear pole face is normal to the beam exit trajectory. The 40^o angle was chosen to enhance beam focusing in the plane perpendicular to the pole faces by the fringing field.[3] In general, a wedge shaped magnet can focus particles in two planes. The uniform gap field, if the bending angle, source and collector distances are properly selected, will focus in a plane parallel to the pole faces. The non-uniform fringing field through its magnetic field component parallel to the pole face can exert a force on particles in a direction normal to the pole face plane. By choosing the proper wedge angle for the source and collector distances established to meet the gap field focusing requirements, this force can cause a focusing of particles at the collector in the plane normal to the pole face. The pole pieces were machined from soft iron with a ¼-inch inset and set screw to attach to the magnet bars. The magnet poles are contained in machined aluminum cups set into the main body of the mass spectrometer. The magnet is thereby free to be removed with the spectrometer under vacuum. The space between the cup faces for beam passage is ½ inch. An angular scale was attached on each side of the magnet. A scribe mark on each magnet bar allows the pole piece orientation to be varied as desired during operation. It was found that best beam focusing occured with the poles oriented as described above. The ion source spool was machined from a section of 4¼-inch ID, 4½-inch OD, type 6061-T6 aluminum pipe and heliarc welded by the Superior Welding Service, Redwood City, California, to the spectrometer cover plate and source flange.

During initial runs of the mass spectrometer it was observed that the heat developed by the ion source was not being dissipated properly. A cooling coil consisting of about ten turns of copper tubing was placed around the source can and cemented in place with a special heat conducting cement.

The electrical circuit for the magnet is shown in Fig. 5. The magnet in the mass spectrometer was powered by a Power Designs Transistorized DC power supply; Model 36100R, 0-36V, 0-10A, using the remote current programming feature of the supply. The supply was connected through a polarity reversing switch to a small patch panel. This panel provided outlets for the connection of the magnet, insertion of an ammeter in the coil circuit, insertion of an X-Y plotter in the coil circuit for continuous record of magnet current during sweeping, and an adjusting potentiometer for remote plotter calibration. Another panel was located adjacent to the power supply on which was mounted a switch to select remote programming, a ten-turn helipot for remote magnet current adjustment, and an on-off switch for a small AC motor used to drive the helipot at a constant speed for use with the X-Y plotter. The sweep speed of the coil current could be varied by changing the motor-helipot drive ratio. This drive consisted of various diameter pulleys on both the motor and helipot shafts connected with an O-ring.

The ammeter in the coil circuit was a Weston DC, Model 45, 0-5A, which was carefully calibrated before the experiment. This ammeter was used to calibrate the X-Y plotter scale which was the source of all current data points. The circuit described allowed careful and accurate sweeping of the magnet current and rapid degaussing of the field after each run with little effort.

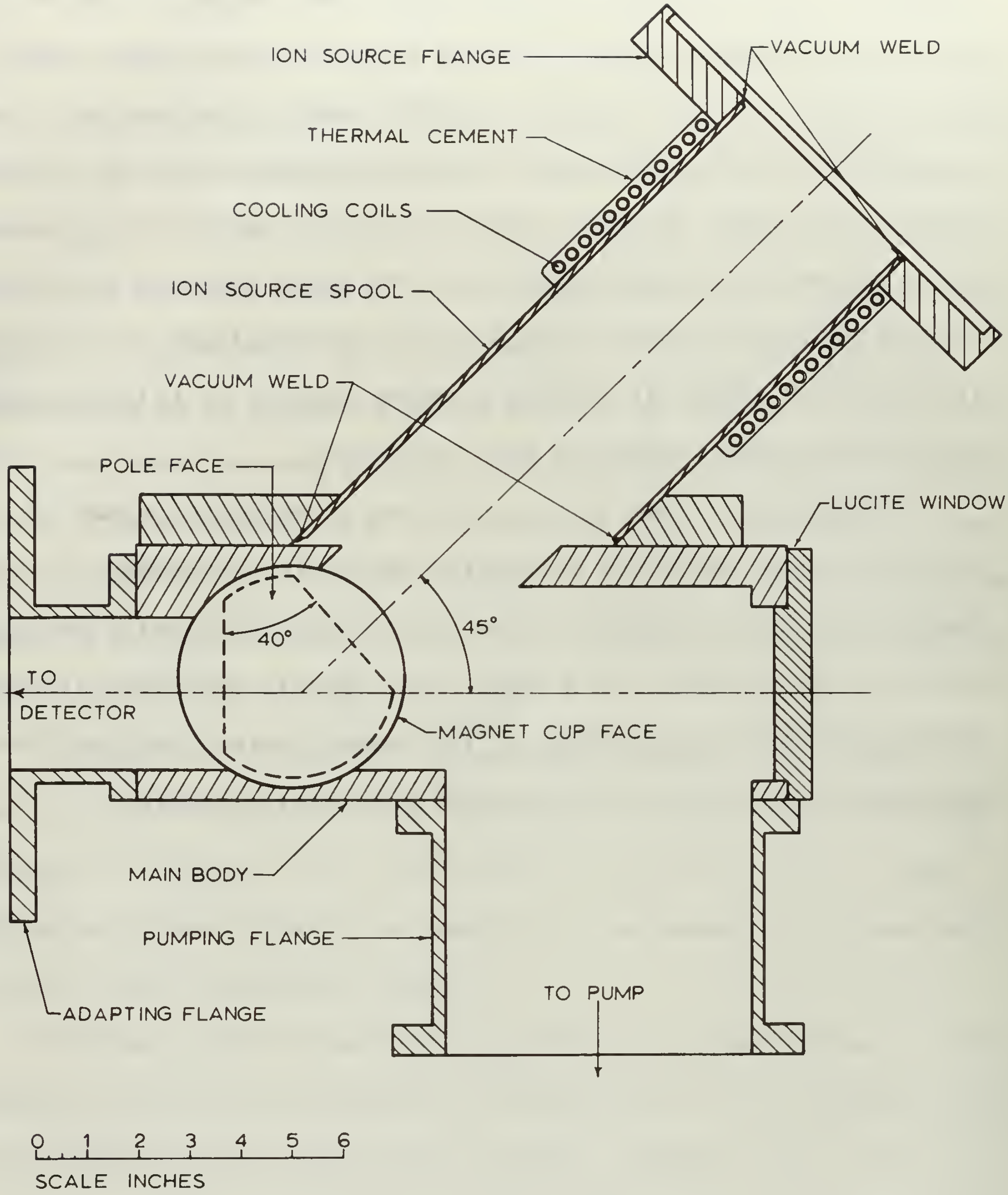

FIGURE 1

CROSS-SECTIONAL VIEW OF MASS SPECTROMETER

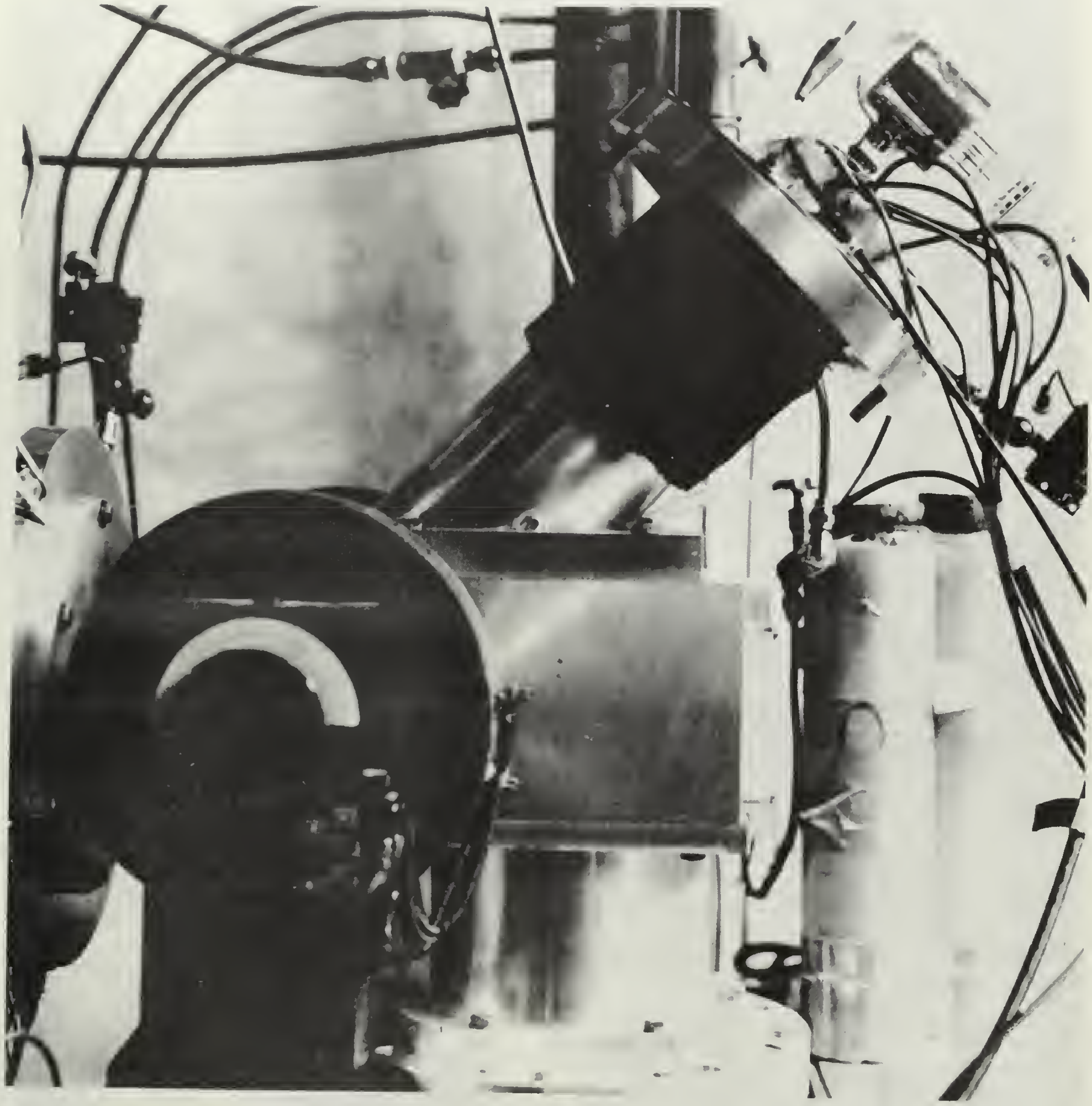

FIGURE 2

SIDE VIEW OF MASS SPECTROMETER

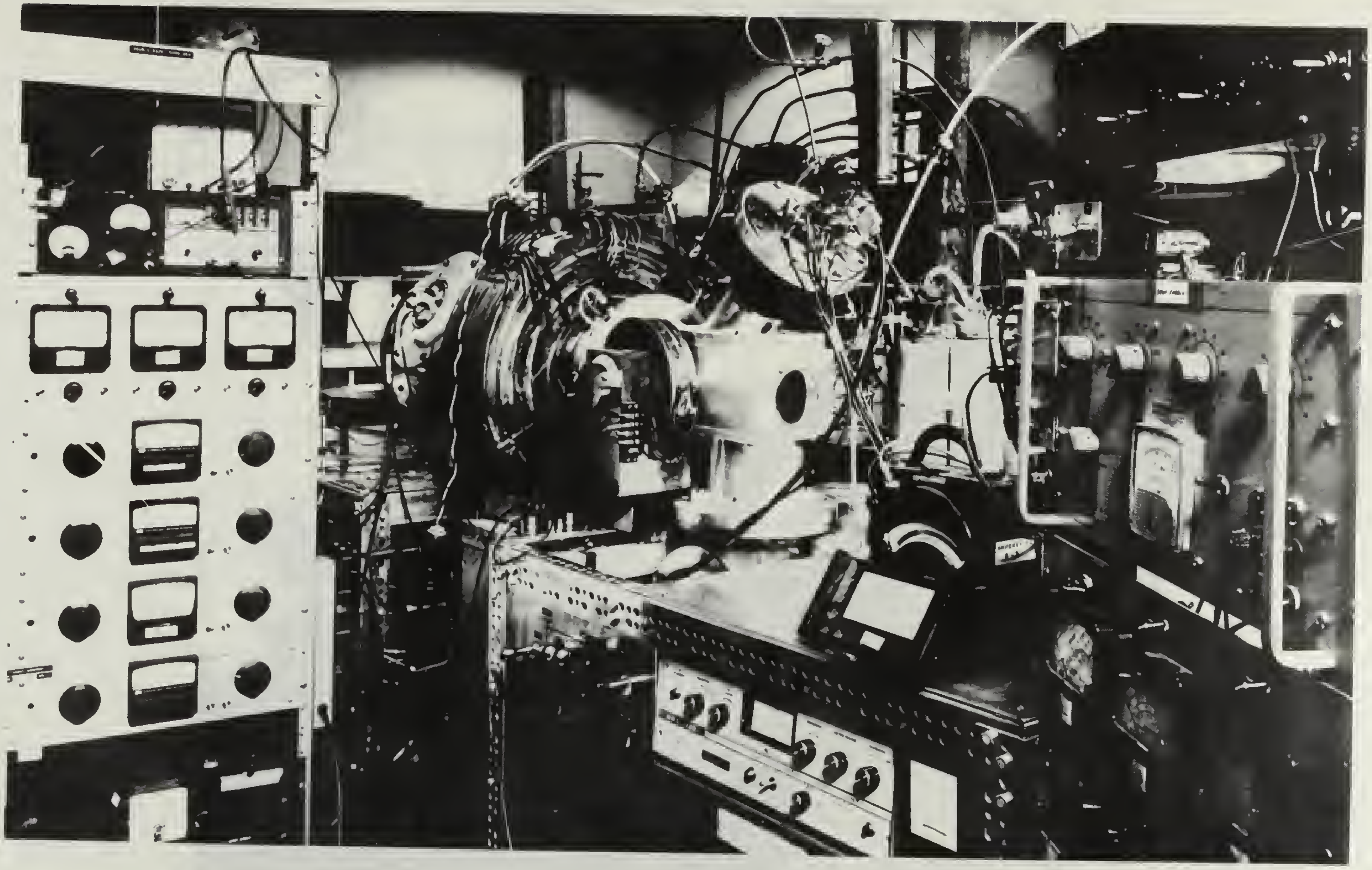

FIGURE 3

MASS SPECTROMETER AND SCATTERING APPARATUS

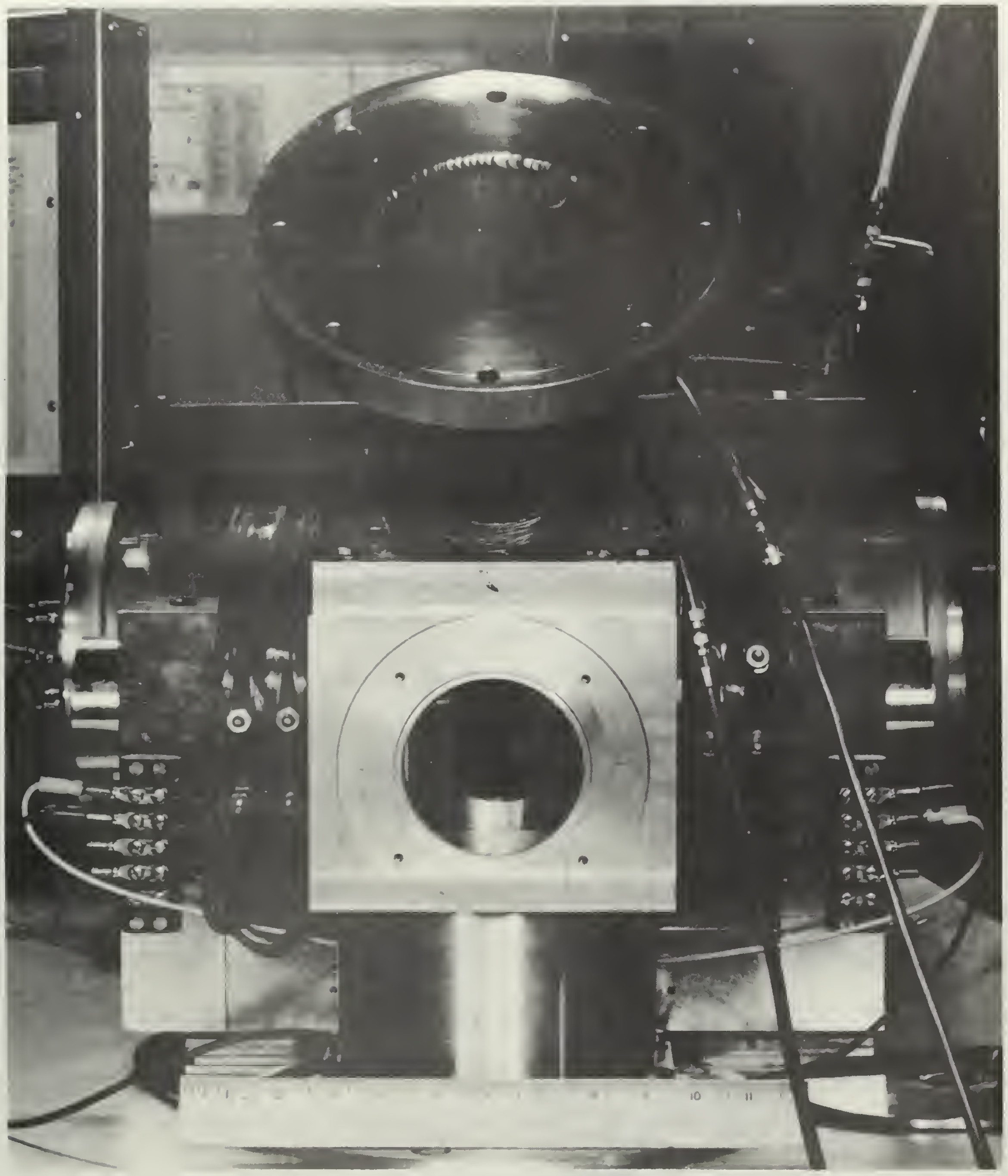

FIGURE 4

REAR VIEW OF MASS SPECTROMETER

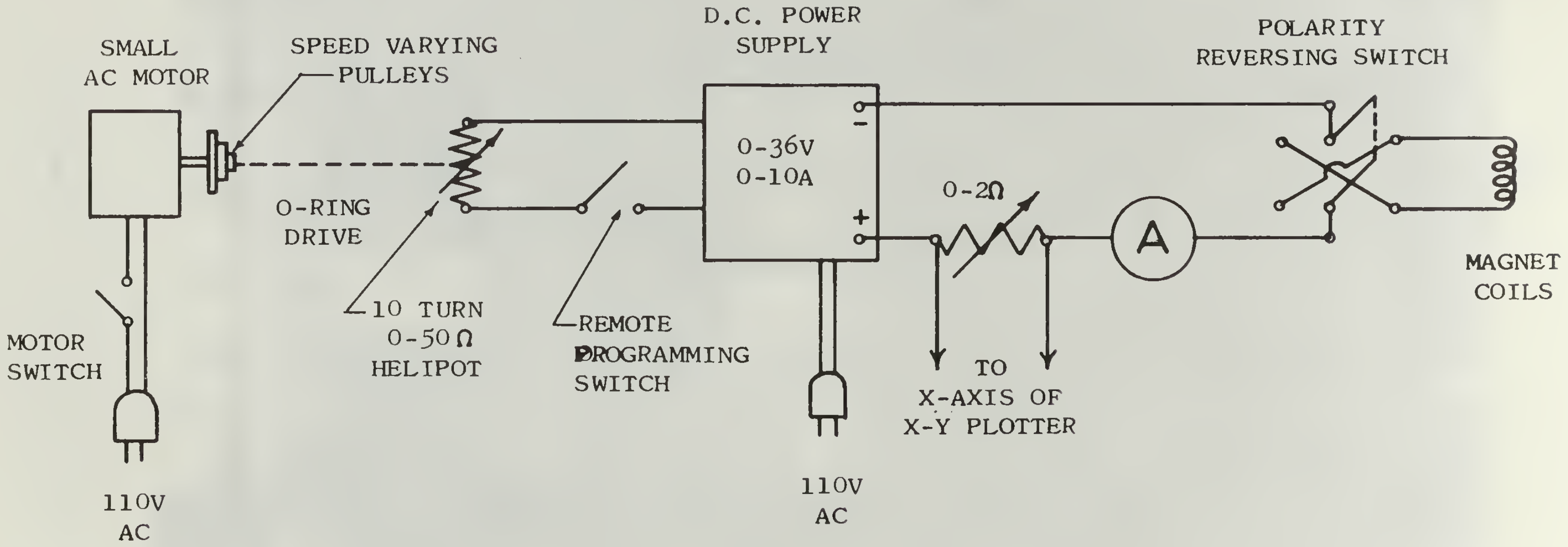

FIGURE 5

SPECTROMETER MAGNET CONTROL CIRCUIT

B. Vacuum System

The vacuum pumping system used in the calibration of the mass spectrometer consisted of a commercially assembled pumping station on which was mounted the mass spectrometer. The spectrometer was connected via an adapting flange to a large chamber containing the detector, energy analyzer, and second set of focusing lenses. Both the detector chamber and vacuum pumping system are described in complete detail, including drawings, by Lambert.[4] Briefly, the vacuum pumping system, assembled by CHA industries consists of a Welsh Duo-Seal 15-cfm mechanical forepump, an NRC 6-inch oil diffusion pump with a 1500 liter/second capacity, stainless steel baffling and a CHA liquid nitrogen trap. The controller is a Cooke Vacuum Products ion-gauge control.

The detector chamber is a cylindrical aluminum can, 10 inches in height and 18 inches in diameter. There are four 3-inch access ports symetrically spaced around the circumference and a removable top. Detector chamber pressure was measured with a Bayard-Alpert type ion gauge mounted on the chamber top. Pressure in the gas source was measured by a NRC ion gauge mounted on the source itself. An NRC ion gauge controller was used for this measurement to allow readings in the range of one to ten microns.

The vacuum pumping system attained vacuums in the 10^{-8} torr range at the liquid nitrogen trap and 10^{-6} torr range in the detector can without baking. These pressures were easily maintained with the lithium source operating. However, the gas source, operating at about 3×10^{-3} torr, caused the detector chamber pressure to rise to about 2×10^{-4} torr. At this pressure the mean free path is still about 10 times the length of ion beam travel. This is adequate for the calibration purposes of the experiment.

Cooling for the oil diffusion pump and for the mass spectrometer source can was provided by a fresh water manifold and distribution system adjacent to the vacuum system.

During operation, the system required little attention and was allowed to operate continuously. An automatic liquid nitrogen trap filler, employing a temperature sensing probe in the trap, ensured continuous trapping. It was necessary to occasionally vent the system and coat all the surfaces exposed to ion beam contact with Aguadag* to overcome charge build up due to the gradual accumulation of an oil coating.

---

* Aquadag is a commerically available colloidal suspension of graphite in water.

C. Gas Ion Source -- Construction

The gas ion source used to produce ion beams from the common laboratory gases operates by extraction of ions from a plasma generated by electron impact ionization.[5] The source, shown in Figs. 6 and 9, consists of a ½-inch diameter helical, 15 mil, tungsten filament concentrically located within a 1-inch diameter helical, 15 mil, tungsten grid. The filament and grid are supported by four 1/16-inch diameter tungsten rods mounted on an inverted 2¼-inch diameter glass press. This assembly measures approximately 5 inches in length. The assembly is mounted inside a stainless steel can, 2½ inches in diameter and 5 inches in length. The base of this source can is mounted via a lavite insulating ring to a 8¼-inch diameter aluminum base plate. The base plate contains the vacuum O-ring for source installation in the mass spectrometer source spool, nine kovar electrical feed throughs, a ¼-inch ID gas inlet pipe with metering valve and an ion gauge mounting fitting.

The beam extraction end of the source can contained initially a ½-inch diameter beam extraction aperture. Mounted over this aperture are a set of three lenses (i.e. an einzel lens configuration) with similiar apertures for beam passage and four beam deflector shims. During the experiment the configuration of the ion source was altered by adding a fourth lens and removing the beam deflectors which were found to be unnecessary with proper source alignment. The holes in the lenses were increased to 1.4 cm to correspond with their individual separations to enhance beam focusing. A reduced extraction aperture of ½ cm was also used in an effort to better confine the gas, reducing system pressures, and improving beam intensities.

Theory of Operation

The gas, injected into the source at pressures in the 10^{-3} torr range, is ionized by electron impact. The electrons are thermally generated by the hot filament ($1800 - 2000^{\circ}C$) and accelerated toward the grid which is held at a positive potential of about 100 volts with respect to the filament. Both the filament and grid are electrically floated on the potential of the source can. When the gas pressure is increased to a critical value the discharge becomes self-sustaining due to the ionization caused by the secondary electrons. The plasma thus generated assumes a potential equal to the most positive potential of its environment, i.e. the sum of the can and grid potentials. The first lens outside the can is held at ground and thereby establishes an electric field which accelerates the escaping ions converting their potential energy to kinetic energy. The discharge in the source is believed to follow the principles of a Townsend discharge.[6]

Considerable investigation of the operating characteristics of this source has been done as a preliminary step in the prosecution of the main scattering experiment. However the reactions which describe the discharge, especially with hydrogen gas, are quite complex and time did not permit investigation of this problem. It will suffice to state that the ion beam constituents and their relative intensities, the total beam intensity and energy are sensitive functions of the source operating conditions; namely gas pressure, grid voltage, filament temperature, and impurities present in the gas. For the purpose of this thesis it was not attempted to analyze these relationships but merely to generate a beam of adequate intensity for detection containing all the ion species possible. The final product, a calibrated mass spectrometer and functional detection apparatus, will permit further investigation into the actual operating parameters of the source.

Operating Techniques

The source was operated by first heating the filament to the required temperature for adequate electron emission. The power required to accomplish this varied between 150 and 250 watts due to filament aging and changing contact resistances within the source. A Kepco Regulated DC Power Supply, Model ICO-45-30M, 0-50V, 0-30A, was used for this purpose although AC power can also be used. A Kepco Voltage Regulated DC Supply, Model 500R-B, 0-600V, 0-300MA, provided the grid potential, while another Kepco supply, Model 605, 0-600V, 0-500MA, provided the necessary can potential. The technique was to place the grid at a potential of 100 volts and slowly increase the filament power until an electron current of about 100 ma was established. The can potential was set so that its value plus the 100 volts on the grid equaled the desired beam energy in electron volts. The gas inlet valve was then slowly opened. When the self-sustaining discharge was reached, the grid current would rapidly rise to some plateau value. An operating grid current of about 175 ma seemed to give near maximum beam intensities. The pressure reading of the ion gage on the source was generally in the 1 to 3 micron range for a self-sustaining discharge for all gases. This however is not the actual gas pressure because the ion gauge reading is correct only for nitrogen gas. A correction factor must be applied to obtain the actual pressure of gases other than nitrogen.

Usually the filament power needed to be readjusted after gas admission to maintain the desired grid electron current. The 100 volt value of grid potential was used to obtain the maximum electron-impact ionization cross section for hydrogen and helium.

Source gases were passed through a liquid nitrogen trap to remove water vapor prior to entry into the source. At can potentials in excess of 500 volts, arcing occured in the source, thus setting a limit on the beam energy available from this source. The lower limit on beam energy is the required grid potential necessary to achieve ionization.

In calibrating the mass spectrometer, the use of an energy measuring device was necessary because of the sensitivity of the beam energy to source gas pressure. A variation in beam energy of over 100 eV at an applied potential of 300 volts could be observed while striking the self-sustaining discharge simply by changing the source gas pressure by one or two microns. Since the operating pressure range falls at the high pressure limit for ion gauge measurement but is too low for thermocouple measurement, large inaccuracies existed in pressure control.

Beam intensities in the range of 10 microamps were obtainable from the gas source, as measured by a collecting plate placed ahead of the magnet poles.

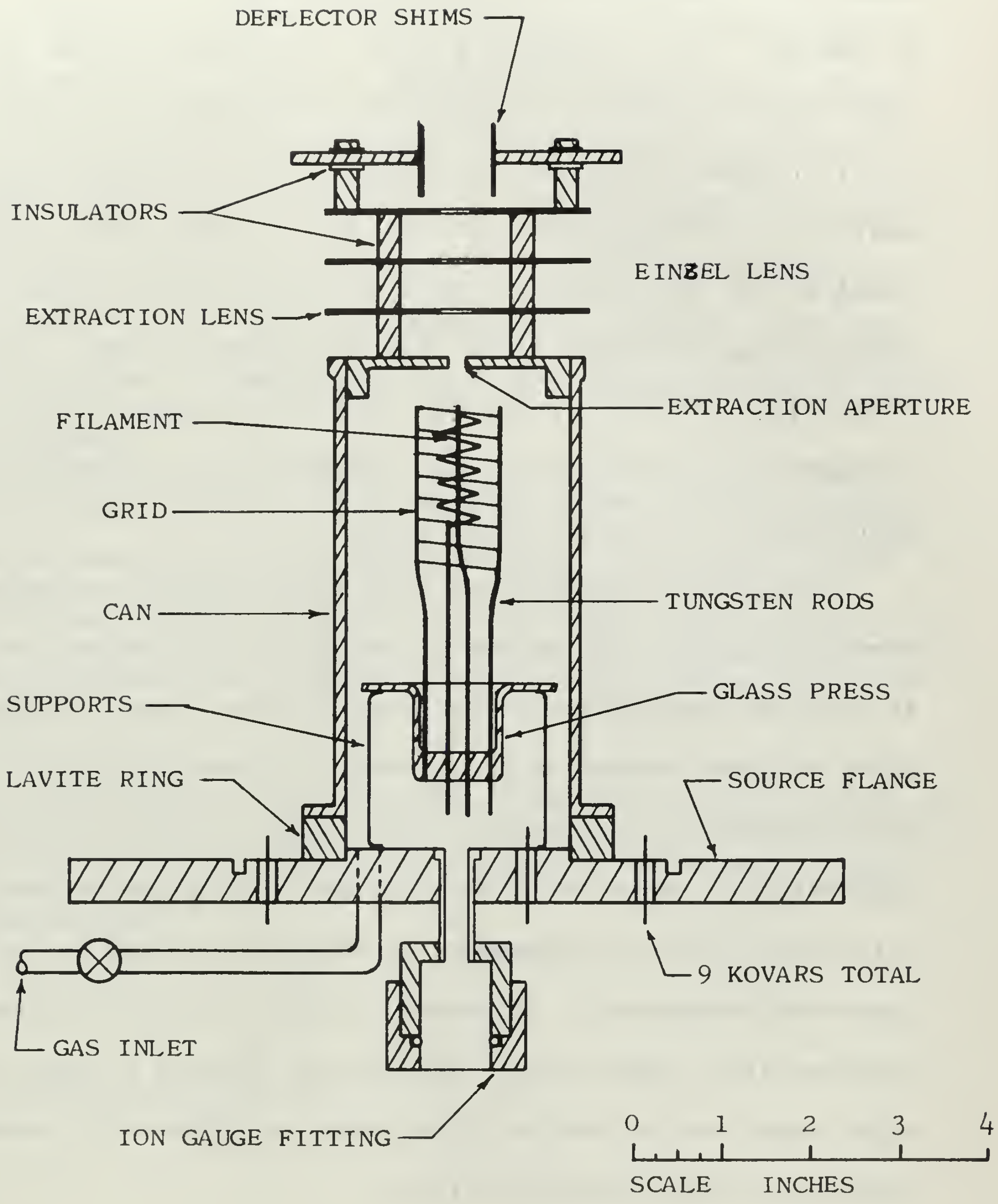

FIGURE 6

GAS ION SOURCE

D. Lithium Ion Source

The lithium ion source used in the calibration of the mass spectrometer was essentially the same source arrangement as reported by Haskell[7] and is shown in Fig. 8. A thermal emitter of lithium ions using the mineral β-eucryptite, manufactured by Spectra-Mat Inc., Freedom, California, was employed as a source of ions. This emitter was enclosed in a heat shield to reduce the filament power required for operation, and mounted on an 8½ inch diameter aluminum flange using stainless steel legs and mounting ring. The flange, as with the gas source, contained the necessary kovar electrical feed-throughs for source operation. Supported over the emitter was an extraction grid and an einzel lens.

An optical pyrometer was used with a mirror arrangement to view through the rear window of the mass spectrometer and obtain the emitter temperature for various filament power settings. A curve of these temperatures vs power is shown in Fig. 7. It was found necessary to determine a new curve for each new emitter as they vary in temperature characteristics from one to another. The value of 1170°C as recommended by Haskell was used as the optimum operating temperature. As shown by Fig. 7 a value of about 90 watts provided this temperature. Both AC and DC type filament power supplies were used at various times with no differences noted in the source operating characteristics.

The emitter was placed at a potential equal to the desired beam energy in electron volts and the extraction grid grounded. The field thus established created the desired beam. Focusing was accomplished with a variable potential on the middle lens while the first and third lenses were held at ground. Lens apertures and spacing were 1.4 cm which, with a "point" source of ions at the extraction lens 1.4 cm from the first einzel-lens, resulted in a collimated beam after focusing. Measurements made prior to mass analysis of the beam indicated a maximum beam intensity of about one microamp. Mass analysis showed that the beam consisted almost entirely of Li^7 with traces of Li^6, Na^{23}, and K^{39}. The sodium and potassium impurities tended to disappear after several hours operation of the source. A search for negative lithium ions showed that none were present.

No particular operating problems were noted with the lithium source in the energy range of 15-800 eV, with the exception that experience showed that the filament must be electrically floated on the emitter potential to prevent shorting of the dielectric in the source cup.

This source proved valuable in the mass spectrometer calibration due to the purity of the beam and the fact that the beam is essentially monoenergetic.[8]

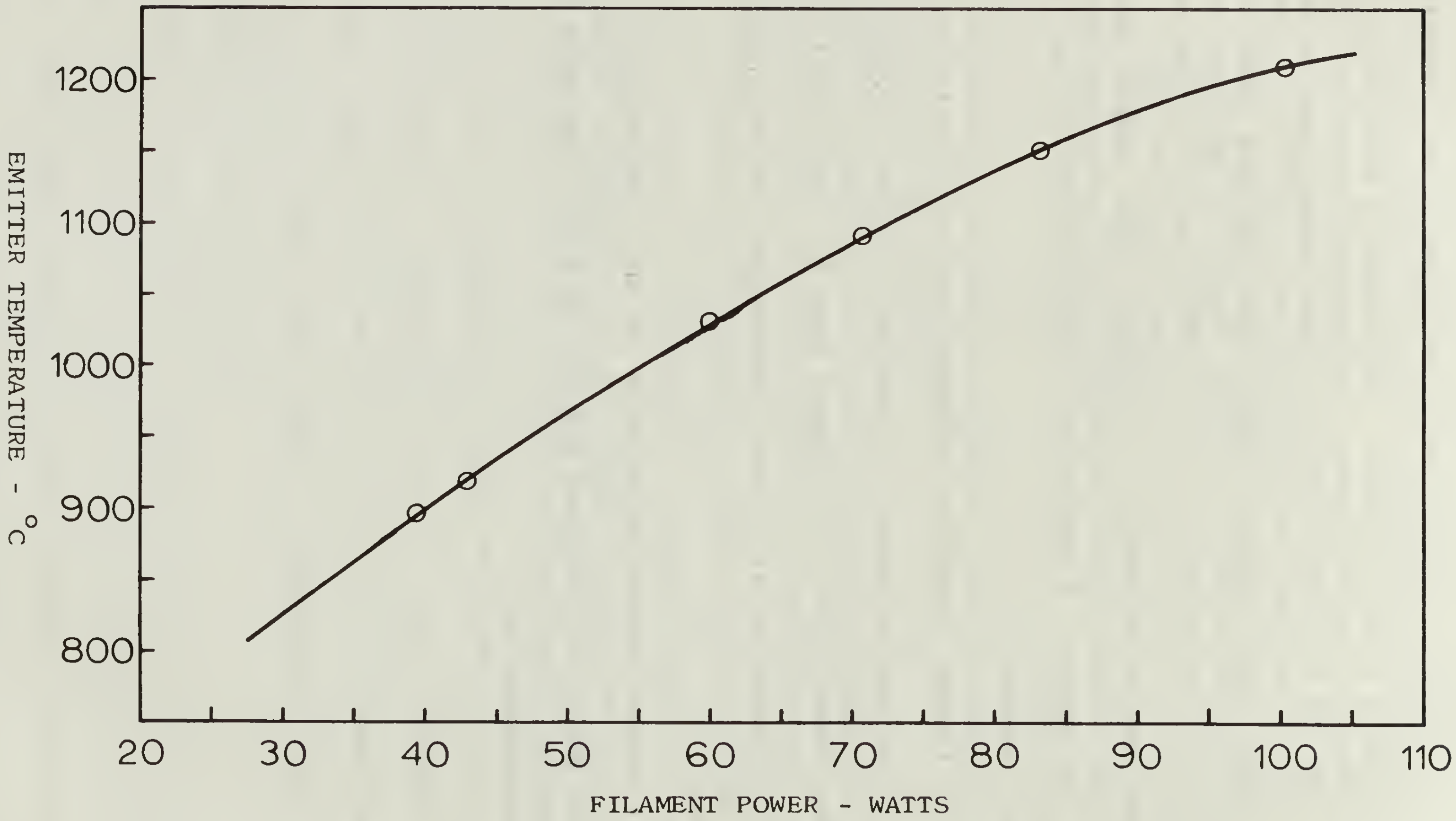

FIGURE 7

LITHIUM EMITTER TEMPERATURE CHARACTERISTIC

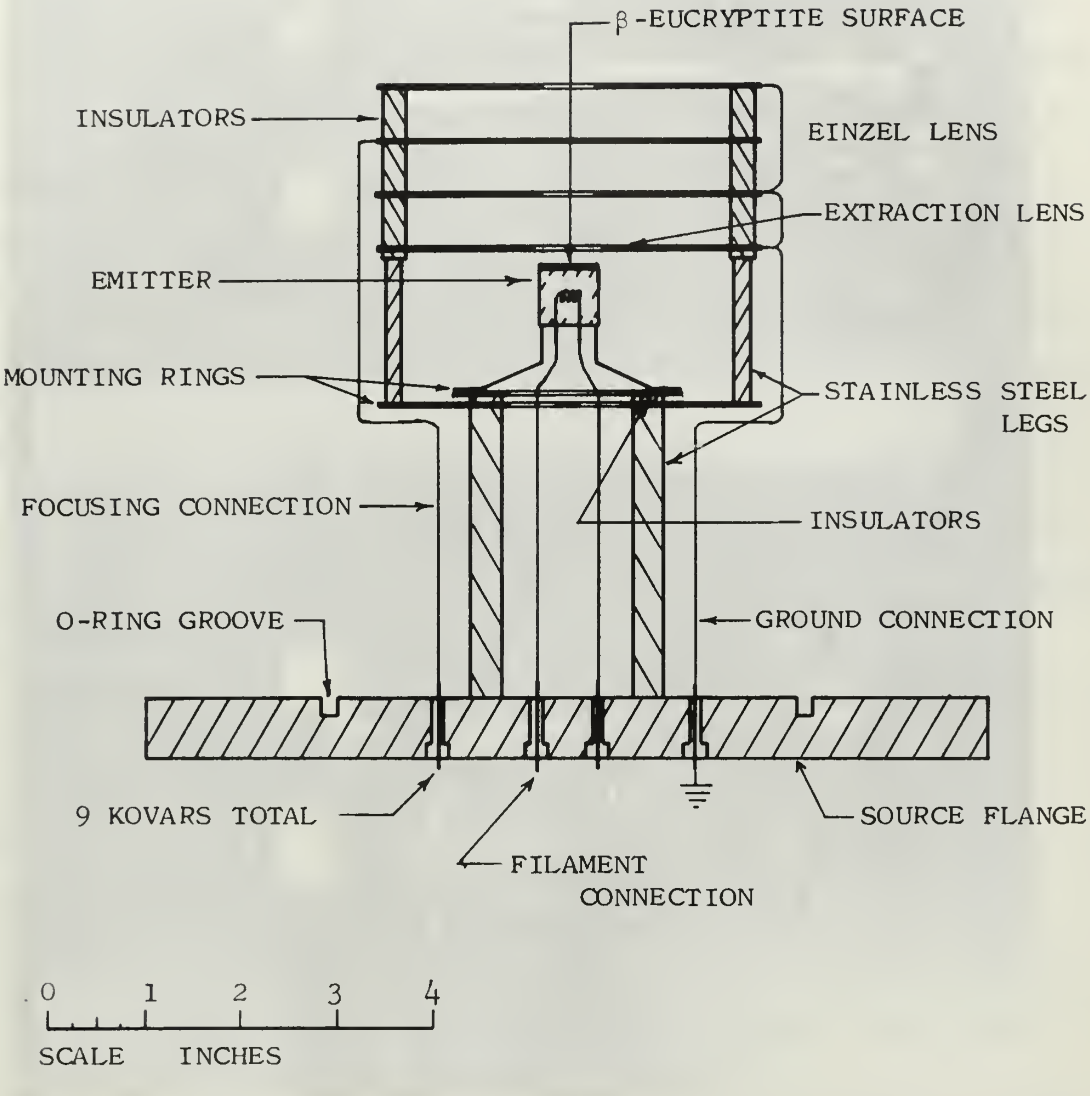

FIGURE 8

LITHIUM ION SOURCE

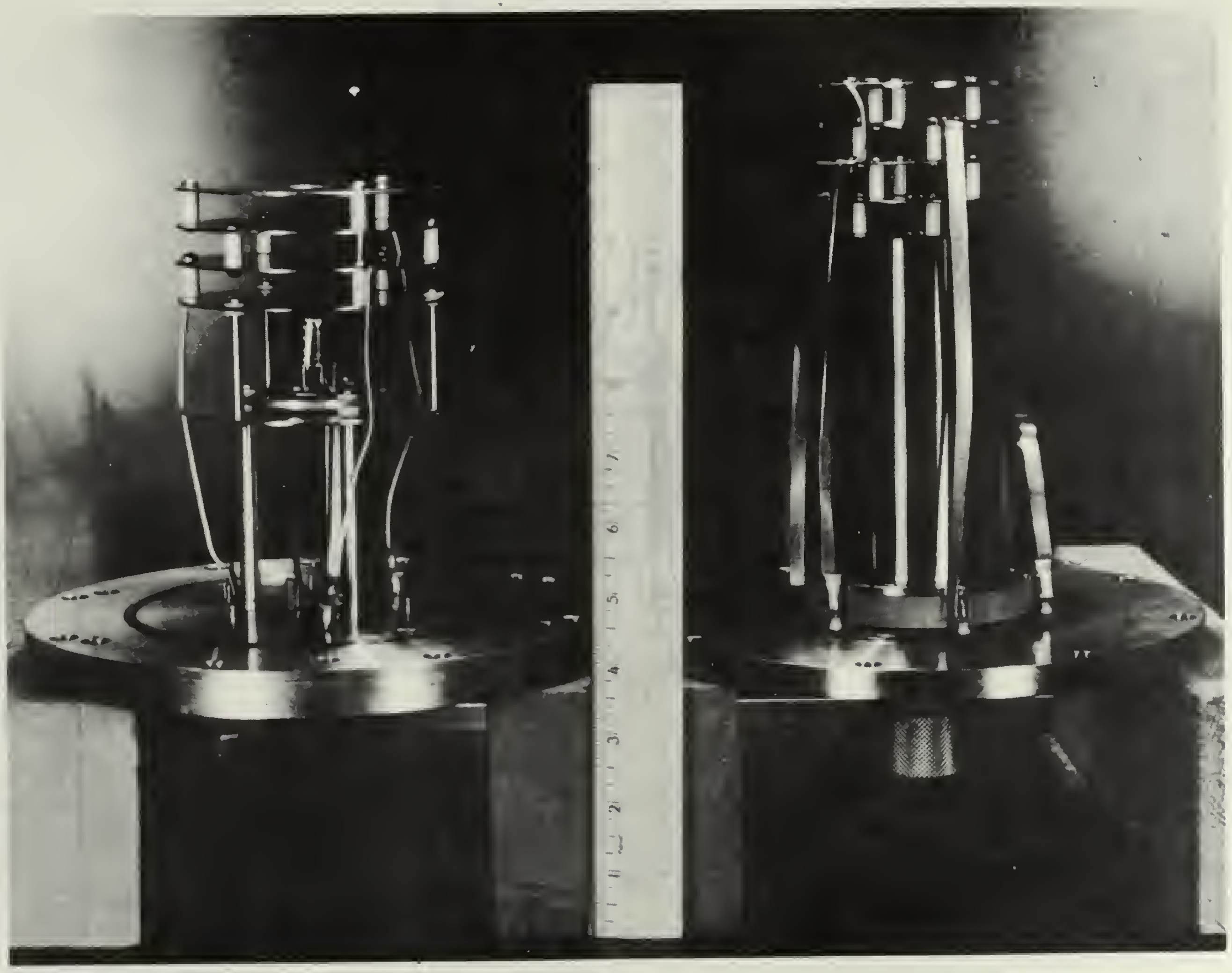

FIGURE 9

EXTERNAL VIEW OF LITHIUM AND GAS SOURCES

E. The Detector

The detector, shown in Fig. 12, employed for measuring the ion beam intensity after mass separation was a simple faraday cup design. The collecting plate was enclosed in a stainless steel cup which contained three electrically separated wire mesh grids of about 90% transparency as shown. The grid closest to the plate was normally held at a negative potential of about 40 volts and acted as a suppressor for secondary electron emmission from the plate. The center grid was normally held at ground potential, and the furthest grid out from the plate which was connected to a variable positive source, established an electric field which could retard the beam for energy analysis purposes. (See Section III.) The entrance to the faraday cup consisted of a variable aperture iris controlable during operation from outside the vacuum enclosure by means of a rod passing through a high vacuum seal.

The entire cup assembly was mounted on a rail within the detector chamber using teflon sliders and was free to be moved along the beam axis, being positioned by the same rod which controlled the iris opening. Besides being thus able to simulate various scattering chamber openings and positions relative to the mass spectrometer, the controlable geometry afforded the opportunity to check that the lens system following the magnet was properly focusing the beam into the cup. An iris opening of 0.3 cm was used for all the calibration runs to coincide with the actual scattering cell aperture. The iris was positioned 29 cm from the exit pole face plane for calibration purposes.

The collecting plate was connected to a Keithly Model 410 Micro-Microammeter for beam detection. The potentials on the grids of the detector and all einzel-lenses were supplied by batteries. The entire detector assembly was aligned with the mass analyzer axis visually using crosshairs and a laser beam oriented on the spectrometer axis. The first attempts at alignment using a surveyors theodolite proved very time consuming and were discontinued when the laser was obtained.

The Keithly also provided a voltage output proportional to the input signal. This output was connected to the Y-axis of the Moseley Autograph Model 2DR-2A, X-Y plotter. Plotting detector signal versus magnet current provided the mass trace which was the desired end product of this project. For purposes of retarding field analysis the X-axis of the plotter was connected to the first grid. The detector operation was satisfactory except in its beam energy determination role which is discussed in Section IV.

F. Energy Analyzer

Due to the large uncertainties encountered with the retarding field measurements a cylindrical capacitor type energy analyzer, shown in Figs. 10 and 11, was used to measure the energy of the beams after mass separation. The particular analyzer used subtended an angle of 127.3°. Hughes and Rojansky[9] have shown that beam focusing in this type analyzer occurs every $\pi/\sqrt{2}$ radians or roughly 127.3°. For a cylindrical analyzer of inside plate radius a, and outside plate radius b, the energy of the particle passing successfully through the analyzer along the central trajectory is given by

$$E = \frac{V}{2 \ln \frac{b}{a}} ,$$

where V is the potential difference between the plates in volts. Using the measured values of a = 5.0 cm and b = 6.0 cm the empirical relation

$$E\ (\mathrm{eV}) = 2.742\ V\ (\mathrm{volts}) \tag{1}$$

was obtained. The resolution of such an analyzer is given by Cook[10] as

$$\Delta E/E = \frac{4}{3}\alpha^2 + \frac{1}{2}\left(\frac{\ell_1 + \ell_2}{\pi r_o}\right)^2 + \frac{w_1 + w_2}{r_o} \tag{2}$$

where ΔE = an apparent energy spread due to analyzer geometry

α = half entrance angle to the analyzer

$\ell_1 + \ell_2$ = length of entrance and exit slits

$w_1 + w_2$ = entrance and exit slit openings

r_o = mean radius of analyzer

The first two terms are fixed by the geometry of the apertures and account for a constant $\Delta E/E$ of 0.8%. At slit widths of .02 cm or greater the third term is the significant term in determining the resolution of the analyzer. The slit width used was 0.05 cm which resulted in a resolution of 2.65% obtained from equation (2).

The alignment of the analyzer is critical and was accomplished by using a small laser to establish the beam axis. A plastic insert was carefully machined to fit between the analyzer plates. At the entrance slit end of this insert was attached a flat mirror. The plane of this mirror was normal to the tangent of the central trajectory through the analyzer. The analyzer was positioned so that the laser beam was reflected back to the source with a single slit diffraction pattern centered over the beam source.

The electrical circuit of the analyzer consisted of a Hewlett-Packard, Model 6110A, DC Power Supply (0-3000V, 0-6MA) connected to the plates as shown in Fig. 10. The potential established by this power supply was accurate to 0.1%. This arrangement with the entrance and exit slits grounded established a symetrical fringing field in the area of the slits and set the center trajectory through the analyzer at ground potential. A grounded circular aperture of one centimeter was provided in front of the entrance slit so that the entrance slit itself could be used as a beam detector. A small collecting plate with fine mesh suppressor grid was used following the exit slit for beam detection through the analyzer.

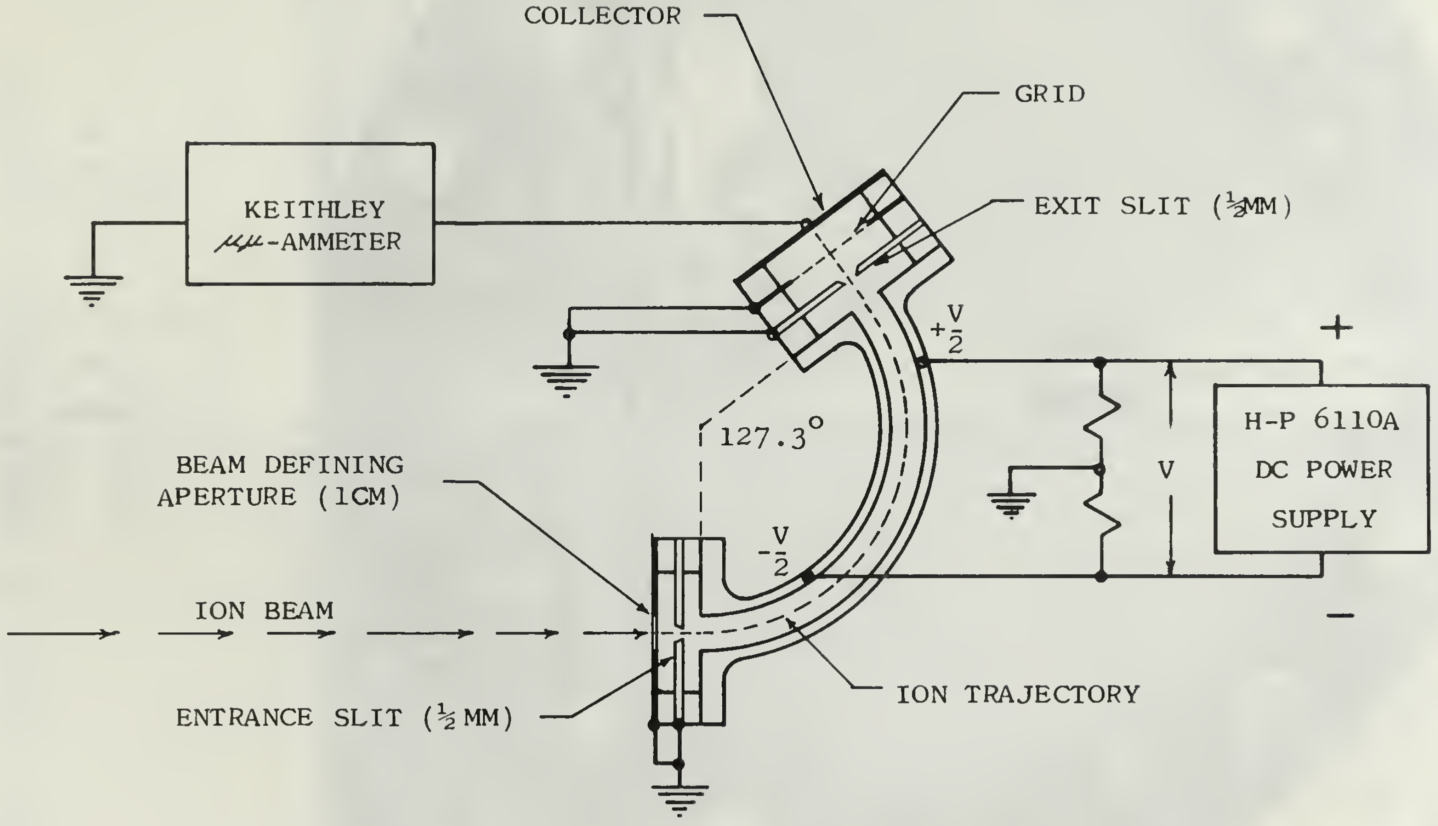

FIGURE 10

SCHEMATIC OF ELECTROSTATIC ENERGY ANALYZER

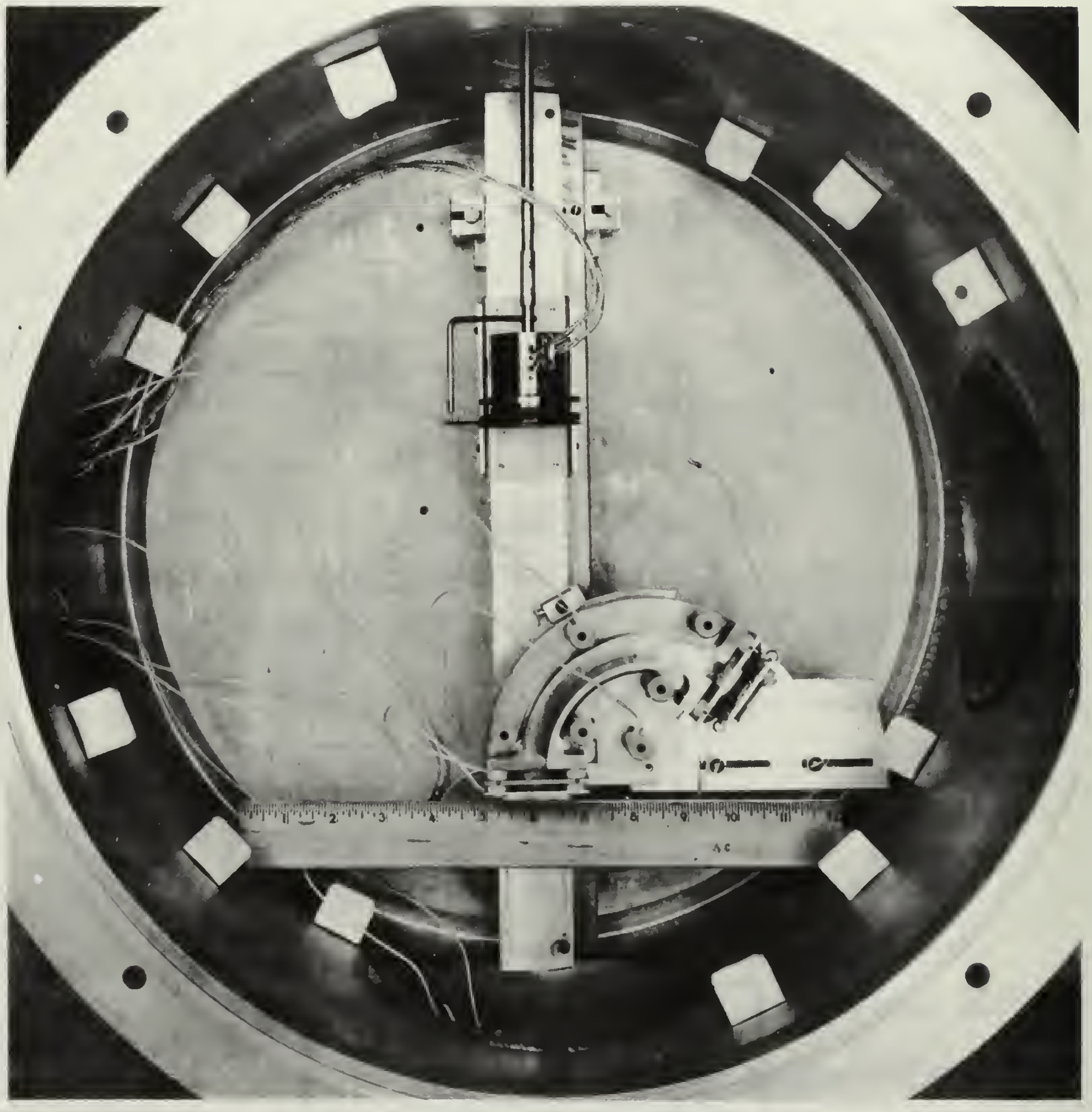

FIGURE 11

BEAM DETECTOR AND ENERGY ANALYZER IN POSITION

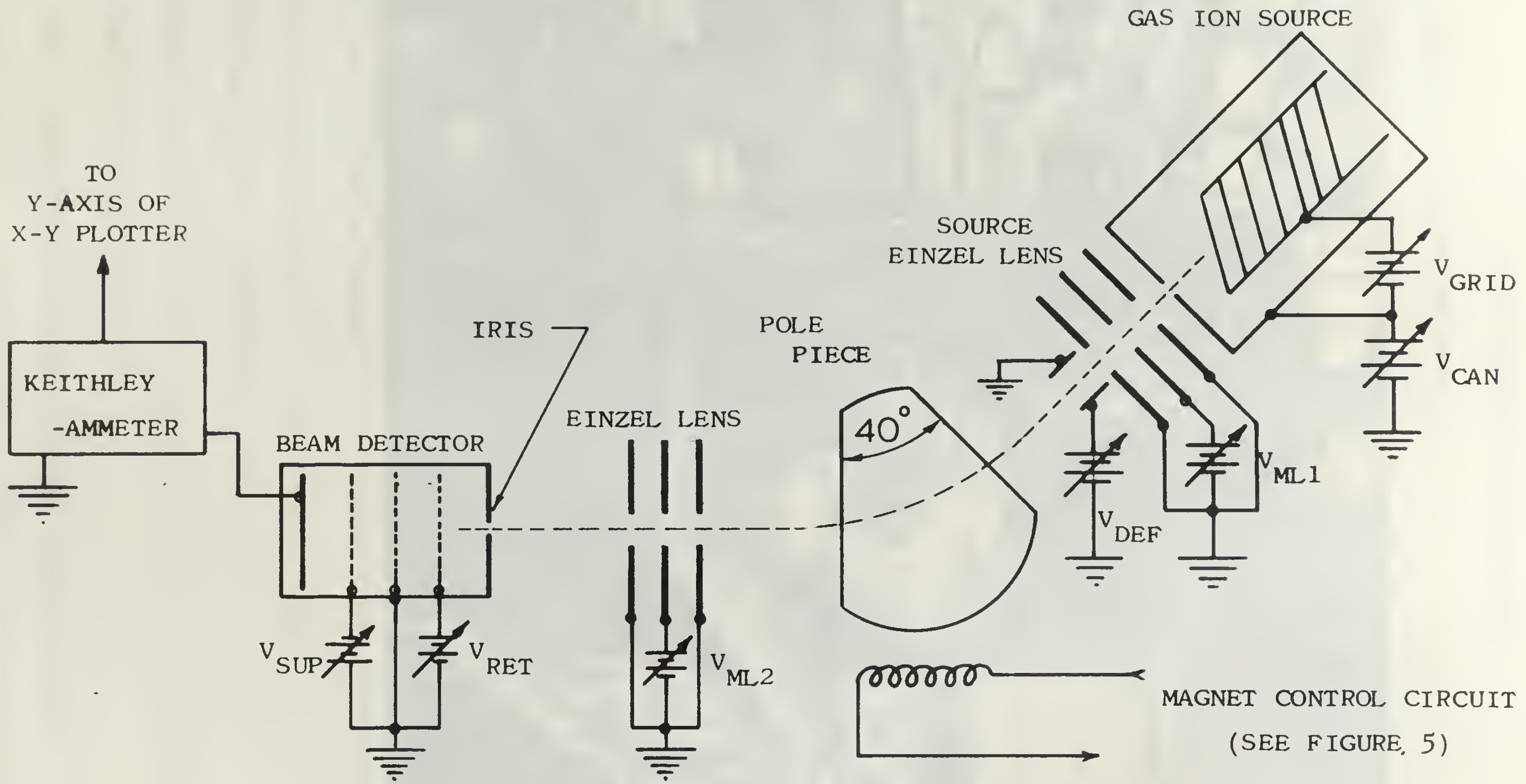

FIGURE 12

SCHEMATIC OF CALIBRATING APPARATUS

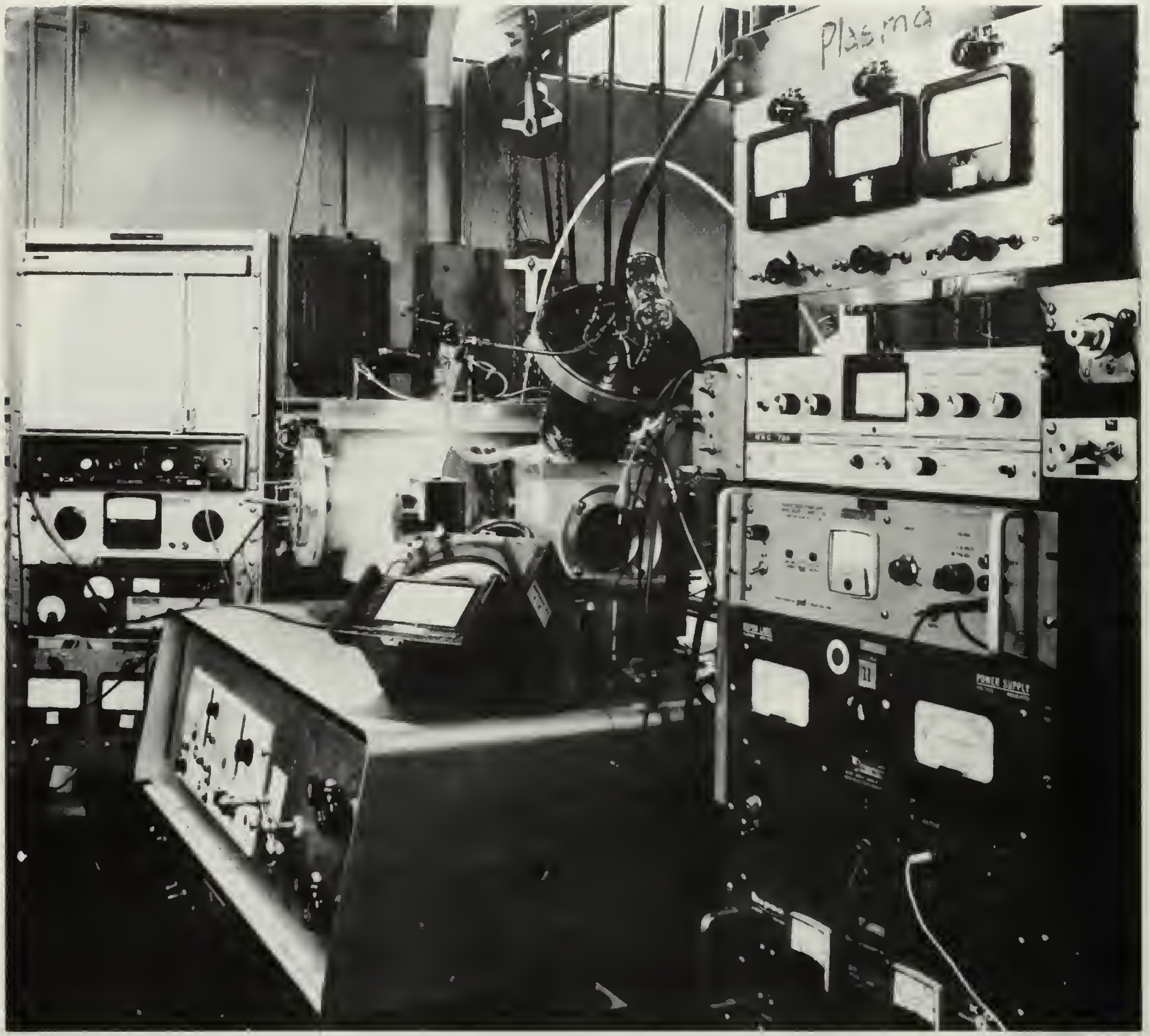

FIGURE 13

EXTERNAL VIEW OF CALIBRATING APPARATUS

III EXPERIMENTAL PROCEDURES

A. Magnetic Field Measurements

The uniform magnetic field between the pole pieces was measured as a function of current in the magnet coils both at the commencement of the calibration phase and again after completion of the data taking. In addition, the fringe field was measured at a constant magnet current as a function of distance from the pole face plane. The fields were measured with a rotating coil gaussmeter which was first calibrated using a large Varian field controlled magnet and a nuclear magnetic resonance probe. The gaussmeter reading proved accurate to within about 3 gauss over the range of fields measured. A small optical bench was used to hold the gaussmeter for the field measurements and allowed accurate positioning of the probe tip for fringe field measurements. Data was taken for various coil combinations in both increasing and decreasing current directions yielding an operational hysterisis loop for the magnet. (Fig. 14) It was decided to make all runs in an increasing field direction and degauss the field between runs to eliminate, as nearly as possible, the effects of hysterisis in the calibration. By trial and error the following degaussing procedure was developed which left residual fields of generally less than 5 gauss:

(1) Following run reduce current to zero.

(2) Reverse polarity and increase current to the maximum value attained in the previous run.

(3) After several seconds reduce the current to about ½ amp.

(4) Slowly reduce current to zero while continually reversing the polarity. At least 20 reversals should be made before reaching zero current.

A least-squares curve fitting program, (see Appendix I), was written and run on the digital computer with the field measurement data yielding the following linear magnetization curve for the case of two coil operation;

$$B = 260.7 I - 27.2$$

where I is in amps and B in gauss.

This equation is valid only for currents greater than 0.25 amps as the magnetization curve is non-linear below this value. Saturation of the field cannot be reached with the number of ampere-turns available on this magnet. Since each magnet coil has the same number of windings, the equation of the magnetization curve for operation with other than two coils is obtained from the above equation by either halving or doubling the coefficient of I depending on whether one or four coils is to be run. As can be seen, a little better than 4 kilogauss field can be attained by the magnet with four coils in operation and maintaining the 8 ampere coil current limit.

The fringe field measurements were also fitted to a curve by the computer program. It was found that a 5th order polynomial gave the best fit of the data points. The fringe field, shown in Fig. 15, is thus described by the equation;

$$B(x)/B(0) = -.00003X^5+.00120X^4-.18415X^3+.13760X^2-.52259X+.91784$$

where

X = distance from the pole face plane in centimeters

B(x) = field value at distance X in gauss

B(0) = uniform field value in gauss.

While a spatial integration of the fringing field could have been performed in establishing particle trajectories, it was felt that other uncertainties in measurement would create larger errors than the use of an approximation of the fringing field. Therefore, in the trajectory calculations the approximation was made that a uniform field existed out to a distance equal to one gap width (3/4 inch) from the pole face plane and the region outside this distance was field free.

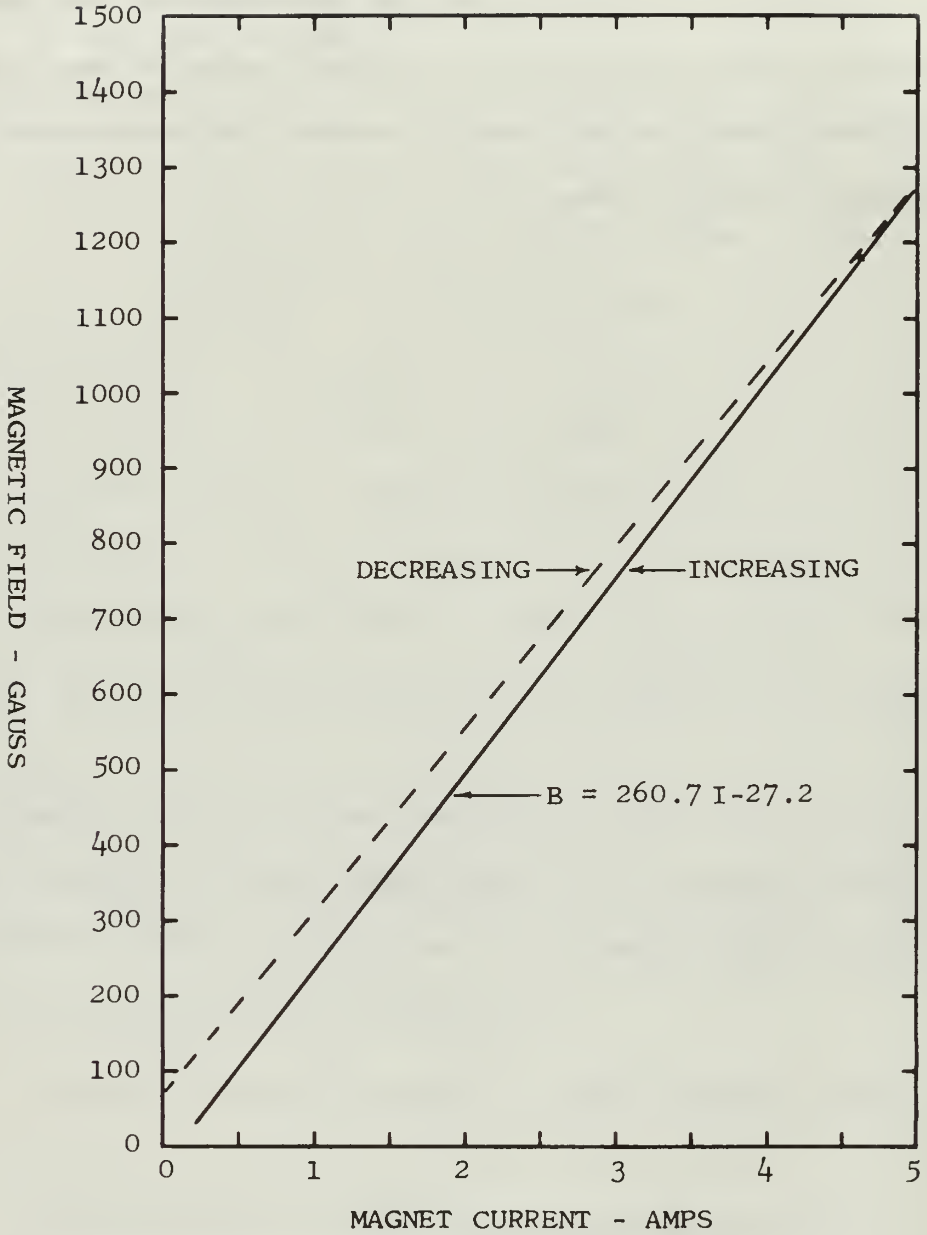

FIGURE 14

SPECTROMETER MAGNETIZATION CURVE

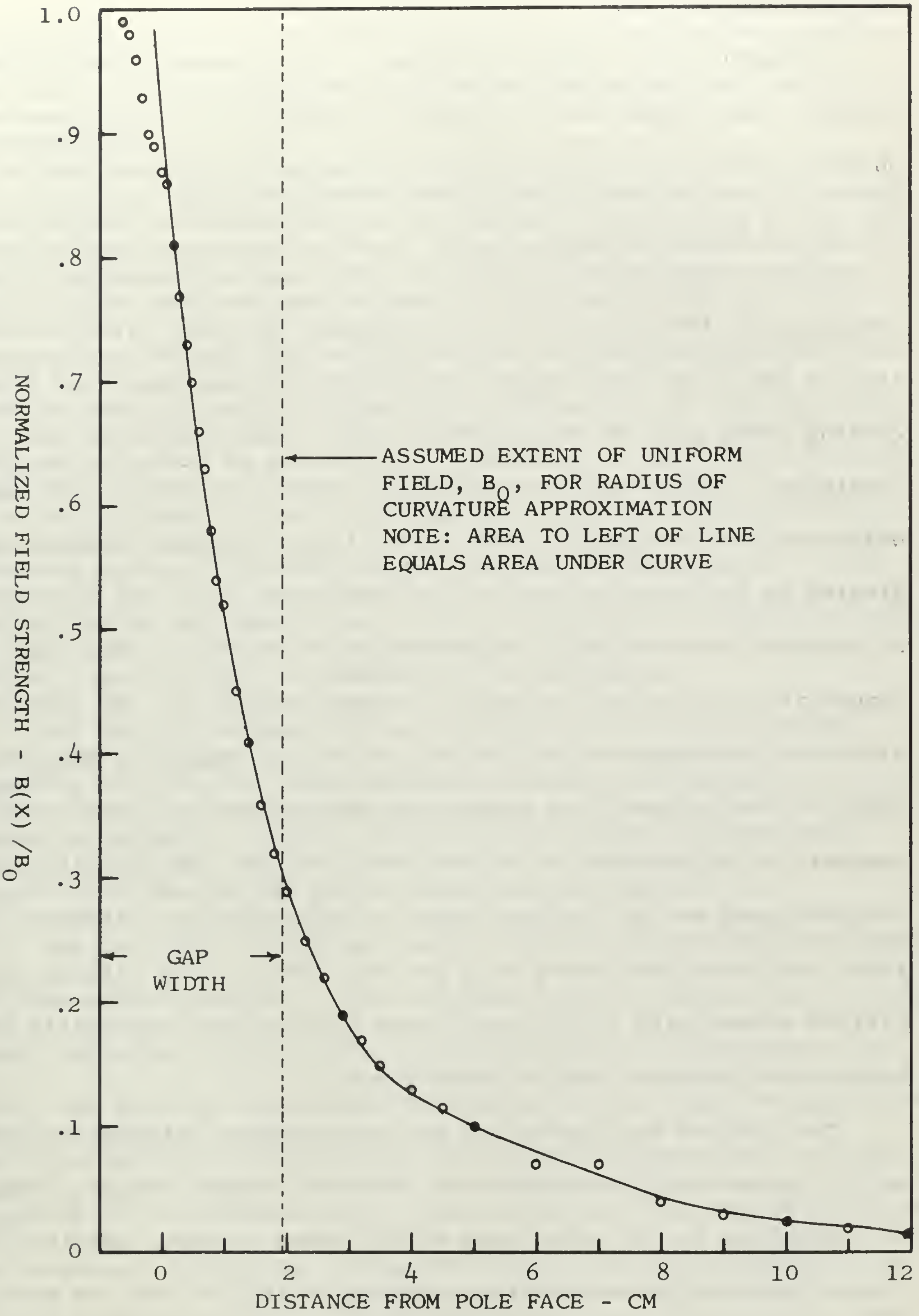

FIGURE 15

SPECTROMETER MAGNETIC FRINGING FIELD

B. Mass Calibration

Throughout the calibration phase of this project the following procedure was established to obtain calibration data. A beam was obtained from the ion source with the energy of interest set with the source potentials. The current in the magnet was varied until a detector signal peak was located. The peak was maximized by beam focusing and fine adjustment of the magnet current. With the system then in focus for this energy, the magnet was degaussed and a recording sweep made of the magnetic field. The X-scale of the plotter was calibrated to read magnet current to within .005 amps while the detector signal from the Keithley Micromicroammeter was plotted on the vertical scale. The resulting trace was a series of detector current peaks corresponding to different mass ions. A composite of three such tracers is shown in Fig. 16. By using a mixture of hydrogen and helium gas in the gas source it was possible to obtain peaks for masses one through four on each trace. However the adjustment of the gas ratio so that the detector signal for each peak was of the same order of magnitude was difficult, and final runs were made using each gas separately. The lithium source yielded essentially only a mass seven peak but was especially useful because the beam was nearly monoenergetic.

The desired end product of the spectrometer calibration was a set of curves which would provide the exact magnet current required to analyze an ion of given mass with a known energy. Additionally the calibration curves obtained experimentally for the low mass ions would be used to check the accuracy of similiar curves generated theoretically and aid in determining the validity of these curves for ions of any mass up the limit of the analyzing power of the spectrometer.

The data analysis process consisted of determining the magnet current from the recorder trace corresponding to each mass peak and pairing this with the beam energy for the run. These data pairs (current and energy) for each mass over all the runs at different energies were fitted to second order polynomials by the computer program described in Appendix I. The computer generated, based on this data, a plot of the resulting least squares curve for each mass and plots of the data points for evaluation purposes. The derivation of the theoretical curves in Appendix II justifies the use of a second order polynomial fit of the data.

The initial attempts at calibration were based on the assumption that the ion beam possessed exactly the energy set on the source potentials. The fit of this data yielded unacceptabley large deviations of the points from the resulting curves.

The next set of runs were made using the retarding field method of beam energy analysis. The technique used to obtain the retarding field curve was to set the mass spectrometer on a particular ion peak. An electron suppression potential of -40 volts was placed on the first grid in the detector. The retarding potential was then supplied to the entrance grid. The X-scale of the recorder was set up to measure retarding voltage while the Y-scale continued to indicate detector current. A typical retarding field curve is shown in Fig. 17 along with the derived energy distribution curve. The rise in beam intensity at potentials close to beam energy is due to the focusing effect of the retarding grid on the beam. The dotted line in Fig. 17 shows the shape of the curve without secondary suppressor potential applied. The curve essentially represents the number of particles with energy greater than v, where v is the retarding field potential. So that

$$N(v_2) - N(v_1) = \text{number between } v_2 \text{ and } v_1 \text{ and}$$

$$\frac{dN}{dV} = \text{number per unit energy interval.}$$

Therefore the energy distribution function can be obtained from the retarding field curve by taking the negative derivative of the curve at successive retarding potentials and plotting the result vs retarding potential which now becomes beam energy in electron volts. The most probable energy of the beam is at the point of steepest slope (i.e. the inflection point) of the retarding field curve. The mean beam energy was taken as the potential required to reduce the initial beam intensity by a factor of two. The least-squares fit of the data using energies as determined by this means offered an improvement over the first runs but considerable variation in data points was still apparent.

To obtain accurate energy analysis the energy analyzer described in Section II-F was installed and a final set of calibration runs made with both sources. Data was taken at increments of about 50 eV starting with the lowest beam energy attainable and continuing up to the highest potentials. The fit of this data yielded a set of usable calibration curves for the ions investigated. These curves are shown in Fig. 18 while the coefficients of the second order polynomials describing them are given in Table I.

Following the calibration runs, the spectrometer was removed from the calibrating apparatus and incorporated into the main scattering experiment as shown in Fig. 3. A measurement of the intensity of a Li^7 beam through the spectrometer to the front face of the scattering cell was made. This was compared with prior intensity measurements made at the same power level when the lithium source was installed on the scattering axis. This comparison indicated that a beam transmission of at least 90% had been achieved with the spectrometer.

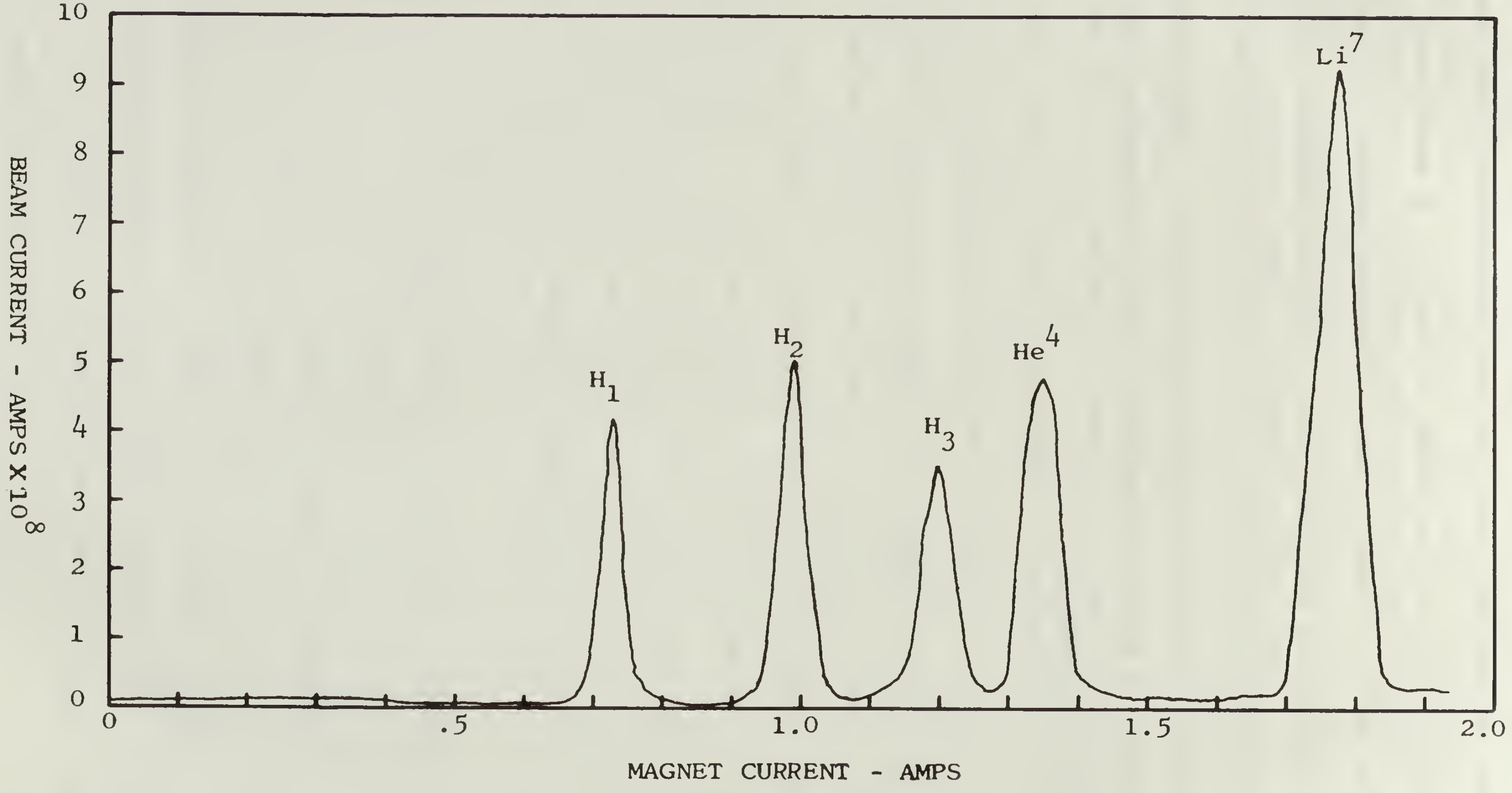

FIGURE 16

TYPICAL SPECTROMETER MASS TRACE AT 300 EV

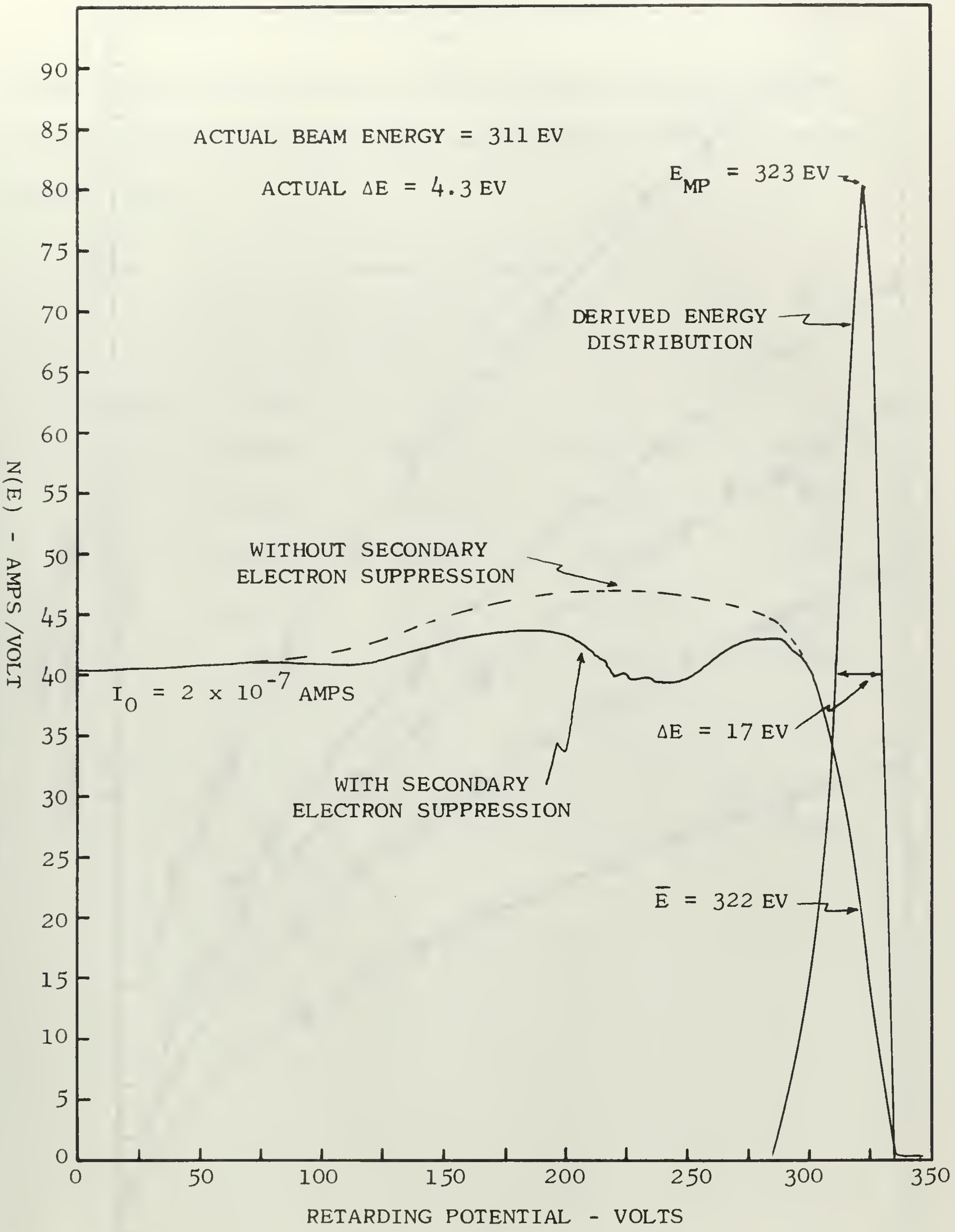

FIGURE 17

TYPICAL RETARDING FIELD CURVE FOR Li^7 ION BEAM

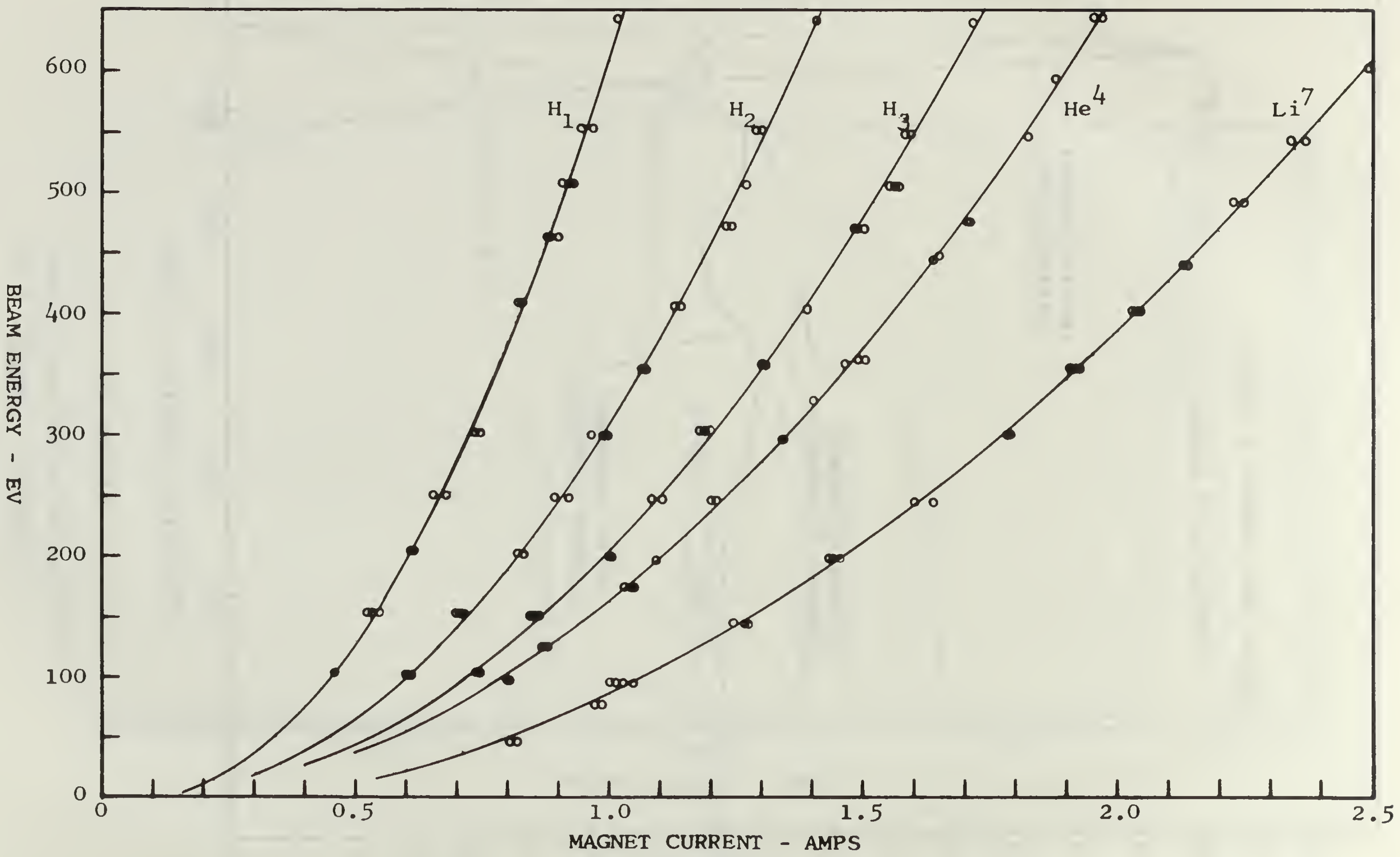

FIGURE 18

SPECTROMETER OPERATION CURVES

TABLE I

Coefficients of the second order polynomials describing the experimentally determined mass spectrometer operation curves of Fig. 18.

General Equation

$$E = C_3 I^2 + C_2 I + C_1$$

SPECIES	MASS	C_3	C_2	C_1
H_1^1	1.00742	706.735	-100.120	3.172
H_2^1	2.01539	365.883	-63.942	6.549
H_3^1	3.02336	229.075	-24.280	0.085
He^4	4.00205	168.476	-3.746	-1.546
Li^7	7.01546	99.169	0.475	-12.716

IV ANALYSIS OF RESULTS

The total of several hundred calibrating runs with the spectrometer confirmed the validity of the degaussing procedure previously described. Mass peak positions under identical energy conditions could be duplicated to within 0.02 amps. While some residual field in either direction can remain after degaussing, its effect on the mass peak position is small enough to permit positive identification of the mass number by its position up to at least mass 20. Where an essentially monoenergetic beam exists, such as from the lithium source, the mass peaks are very sharp, yielding a spectrometer resolution $\Delta m/m$ of about 40 with the present beam aperture arrangement.[11]

As previously stated, the initial attempt at calibration using an assumed beam energy gave poor results. The primary reason for this is that the gas ion source generates a beam whose energy is highly dependent on the gas pressure within the source. Although the sharpest energy variation occurs when the pressure increases to the point of striking a self-sustaining discharge, enough variation is still present beyond this point to cause significant uncertainty in the beam energy. Measurements made with the electrostatic analyzer on the lithium ion beam indicated that the kinetic energy of the beam equaled the applied potential.

The energy measurement results obtained with the retarding field analyzer were somewhat discouraging and certainly misleading. For beam energies greater than about 100 eV, this method of analysis yielded mean energies that were about 7% too large and gave energy spreads that were too great by as much as a factor of 4. Simpson[12] presents a fairly complete analysis of retarding field analyzers of various geometries. He states that for the plane parallel plate type analyzer with an entrance aperture, one can expect to find an energy spread, ΔE, due to the incoming beam divergence and the additional divergence caused by the lens effect of the entrance aperture. Since the retarding field potential barrier can act only on the kinetic energy associated with the axial momentum of the beam, cut-off will start at an indicated energy less than the lowest energy present in the beam. Simpson's relationship

$$\frac{\Delta E}{E} = \frac{r_o^2 (p + 4d)^2}{p^2 \, 16d^2}$$

where

r_o = radius of entrance aperture

p = distance of aperture to image point of source

d = retarding grid to aperture distance in analyzer

yields for this analyzer a value of 0.25%. The resolution actually observed was about 3.8%.

Obviously a rather large discrepancy exists between the predicted analyzer performance and that which was observed. The only plausiable explanation lies in the fact that the ions which are decelerated to very low energies, although not completely retarded, will be subjected to random electric fields within the detector. The effect of the random electric fields is to give too large an energy spread. The fact that the average energy measured was always too high indicates an additional systematic error, the nature of which is not understood at this time.

Future use of the detector as an energy analyzer will require further investigation into this problem. A possible solution is to place the retarding potential on the collecting plate itself or to install additional grids within the detector cup.

The energy measurements made with the 127° electrostatic analyzer are believed to be quite good. The resolution of 2.6% as stated in Section II-F actually represents an upper limit on its true value. It presupposes, for instance, a beam diameter greater or equal to the entrance slit length. Based on the results obtained with the lithium source it is felt that the true resolution was better than 1% for these measurements. An indication of the accuracy of the final data was obtained by computing the effective radius of curvature in the magnetic field for each data pair based on the established magnetization curve and the relationship

$$r = \frac{\sqrt{2mE}}{qB}$$

All of the computed radii were averaged to yield a value of 15.34 ± .15 cm. The geometrically measured radius based on the field assumption discussed in Section III-A has a value of 15.35 cm. It is therefore concluded that the spectrometer operation curves of Fig. 18 are indeed valid and may be used with assurance if the previously described magnet degaussing procedure is followed.

A set of theoretical curves for the spectrometer operation for masses up to number 40 were constructed using the analytical procedure described in Appendix II. These curves are based on the field magnetization curve and the radius of curvature. Agreement with the experimentally determined curves for the ions of hydrogen, helium, and lithium is within the previously stated error for current and energy. (E ± 1%, I ± .02 amps.) The coefficients defining each curve are listed in Table II. These curves may be used to predict the position of any mass peak, for a singly charged ion, up to mass 40. If the current needed to analyze a given mass exceeds 5 amps it is recommended that four magnet coils be used, reducing the required current to one half of its two-coil value.

If the mass spectrometer is to be used to analyze the mass composition of an unknown beam the following simplified procedure for mass number identification is offered:

(1) Make a sweep of the field recording peaks versus magnet current on an X-Y plotter.

(2) Use the calibration curves as given in Fig. 18, or construct curves using the coefficients from Table II for known mass numbers in the sample, to determine the mass numbers of at least two mass peaks on the trace.

(3) On the trace, plot as an ordinate over each known peak the square root of its mass number. All points will fall on a straight line if the assumed mass numbers are correct.

(4) The value of the ordinate over each remaining unknown mass peak is equal to the root of the unknown mass number.

The advantage of this procedure is that if the identity of two peaks is known, then no particular current - field relationship need be maintained, and no degaussing is necessary. Quite good results were obtained using this procedure in identifying Na^{23} and K^{39} impurities in a beam consisting primarily of Li^6 and Li^7 ions.

BIBLIOGRAPHY

1. Bates, D.R., Cook, C.J., and Smith, F.J., "Classical Theory of Ion-Molecule Rearrangement Collisions at High Impact Energies", Proceedings of the Physical Society, v. 83, 1964: 49-57.

2. Feist, E.P., "Classical Calculation of the Differential Cross Section for Scattering of Hydrogen Molecular Ions from Heavy Atoms", Thesis (MS) NPGS, Monterey, California, June 1967.

3. Camac, Morton, "Double Focusing with Wedge-Shaped Magnetic Fields", Review of Scientific Instruments, v. 22, 1951: 197-206.

4. Lambert, Walker W., "Production and Analysis of Lithium Ion Beams in the Low Electron Volt Region", Thesis (MS) NPGS, Monterey, California, 1963.

5. McDaniel, Earl W., Collision Phenomena in Ionized Gases, John Wiley & Sons, New York, 1964: Chap. 5.

6. Brown, Sanborn C., Introduction to Electrical Discharges in Gases, John Wiley & Sons, New York, 1966: Chaps 6 and 13.

7. Haskell, Hugh B., "Investigation of a Low Energy Alkali Ion Gun", Thesis (MS) NPGS, Monterey, California, 1965.

8. Haskell, Hugh B., Heinz, O., and Lorents, D.C., "Multistage Gun for Production of Low Energy Ion Beams", Review of Scientific Instruments, v. 37, 1966: 607-614.

9. Hughes, A. Ll., and Rojansky V., "On the Analysis of Electronic Velocities by Electrostatic Means", Physical Review, v. 34, 1929: 284-290.

10. Cook, C.J., "A Very Low Energy Electron Accelerator", Stanford Research Institute Technical Report, December 17, 1959.

11. Halliday, David, Introductory Nuclear Physics, John Wiley & Sons, New York, 1955: 246.

12. Simpson, J.A., "Design of Retarding Field Energy Analyzers", Review of Scientific Instruments, v. 32, 1961: 1283-1293.

13. McCracken, D.D., and Dorn, W.S., Numerical Methods and Fortran Programming, John Wiley & Sons, New York, 1964: 262-266.

APPENDIX I

A Fortran computer program was written which performs a least-square curve fitting of a given order polynomial to the given data points.[13] The mathematics of this program are as follows:

It is desired to minimize the function

$$S = \sum_{i=1}^{N} (y_i - y_i')^2 \tag{1}$$

where N is the number of (x_i, y_i) data points given and y_i' is a value of y determined from a computed functional relation y(x). The functional relation thus minimizing Eq. (1) is known as a least squares fit of the data.

Assuming that the functional relation y(x) can be expressed as an mth order polynomial

$$y_i' = C_1 + C_2 x_i + C_3 x_i^2 + \cdot\cdot\cdot\ C_{m+1} x_i^m\ , \tag{2}$$

the C_j's can be found which will minimize S as follows.
Substituting (2) into (1) gives

$$S = \sum_{i=1}^{N} (y_i - C_1 + C_2 x_i + C_3 x_i^2 + \cdot\cdot\cdot\cdot\ C_{m+1} x_i^m)^2 \tag{3}$$

By taking the partial derivative of S with respect to each of the C_j's and setting equal to zero, we obtain a set of normal equations of the form

$$\begin{array}{lllll} N\,C_1 & + \Sigma\, x_i\, C_2 & + \cdot\cdot\cdot\cdot\cdot & + \Sigma\, x_i^m\, C_{m+1} & = \Sigma\, y_i \\ \Sigma\, x_i C_1 & + \Sigma\, x_i^2\, C_2 & + \cdot\cdot\cdot\cdot\cdot & + \Sigma\, x_i^{m+1} C_{m+1} & = \Sigma\, x_i y_i \\ \vdots & \vdots & \vdots\ \vdots & \vdots & \vdots \\ \Sigma\, x_i^m C_1 & + \Sigma\, x_i^{m+1} C_2 & + \cdot\cdot\cdot\cdot\cdot & + \Sigma\, x_i^{2m} C_{m+1} & = \Sigma\, x_i^m\, y_i \end{array} \tag{4}$$

For a polynomial of degree m there are m+1 unknown coefficients and independent equations. The set of equations can be expressed in matrix notation as

$$[A]\,[C] = [B] \qquad (5)$$

where

$$A = \begin{bmatrix} N & \Sigma x_i & \Sigma x_i^2 & \ldots & \Sigma x_i^m \\ \Sigma x_i & \Sigma x_i^2 & \Sigma x_i^3 & \ldots & \Sigma x_i^{m+1} \\ \vdots & \vdots & \vdots & \ddots & \vdots \\ \Sigma x_i^m & \Sigma x_i^{m+1} & \Sigma x_i^{m+2} & \ldots & \Sigma x_i^{2m} \end{bmatrix}$$

a square matrix of order m+1, and

$$C = \begin{bmatrix} C_1 \\ C_2 \\ \vdots \\ C_m \end{bmatrix} \qquad B = \begin{bmatrix} \Sigma y_i \\ \Sigma x_i y_i \\ \Sigma x_i^2 y_i \\ \vdots \\ \Sigma x_i^m y_i \end{bmatrix}$$

column matrices of order (m+1) x 1.

The solution of equation (5) is found by inverting A, since

$$[C] = [A]^{-1}[B]$$

The general curve fitting program reads a value of m, N, and the N-element data array into the computer. It calculates the elements of the A and B matrices in a subroutine. The A matrix is inverted by the method of Gauss in a standard computer library subroutine (GAUSS3). The A^{-1} and B matrix product is performed and the result is a required array of coefficients of equation (2) to satisfy the least-squares criterion.

The program was designed to generate as many points as desired along the least-squares curve and to plot these points as a smooth curve in a graphical output. The original data points are also plotted for visual inspection of the quality of fit.

APPENDIX II

The theoretical curves for the operation of the mass spectrometer were obtained by equating the Lorentz acceleration of the particles in a uniform magnetic field to the centripetal acceleration due to the curved particle trajectory and solving for energy in terms of magnet current.

$$\vec{F} = q(\vec{v} \times \vec{B}) = \frac{mv^2}{r_o} \frac{\vec{r}}{|r|} \tag{1}$$

Since the particle velocity vector and the magnetic field direction are at all times perpendicular,

$$q\ v\ B = \frac{mv^2}{r_o}\ . \tag{2}$$

Since the kinetic energy is given by

$$E = \tfrac{1}{2}\, mv^2, \tag{3}$$

we have on substitution

$$E = \frac{(r_o\ q\ B)^2}{2m}\ . \tag{4}$$

Taking r_o as 15.35 cm, which is based on the approximation that the field is uniform out to one gap width from each pole face and zero elsewhere, and considering only singly charged ions,

$$E = \frac{0.0113695}{m} B^2, \tag{5}$$

where

B is in gauss

E is in electron volts

m is in atomic mass units.

The coefficient of B^2 in equation (5) has been tabulated in Table II as K_1.

The least squares fit of the magnetic field measurements data yielded the relationship between field and current as

$$B = 260.69114\ I - 27.21712 \tag{6}$$

Substituting this relation into (5) gives an equation of the form

$$E = C_3\ I^2 + C_2\ I + C_1 \tag{7}$$

Table II tabulates these C_i coefficients for various atomic and molecular ions up to atomic mass 44. When used as the values for the C_i's in (7), these coefficients describe the predicted second order operating curves for the mass spectrometer.

An equation of similiar form as (7) but with different coefficients can be used to describe the operation curves for the analysis of ions of multiple charge. The charge, q, in equation (4) is assigned the appropriate value to reflect the ion charge state and the coefficients computed as above.

TABLE II

Coefficients of the second order polynomials describing the theoretically determined mass spectrometer operation curves from Appendix II.

General Equations (Singly ionized particle)

$$(1) \quad E = K_1 B^2$$

$$(2) \quad E = C_3 I^2 + C_2 I + C_1$$

SPECIES	MASS	$(K_1 \times 10^3)$	C_3	C_2	C_1
H_1^1	1.00742	11.28575	766.978	-160.151	8.360
H_2^1	2.01539	5.64134	383.385	-80.053	4.179
H_3^1	3.02336	3.76056	255.567	-53.364	2.786
He^4	4.00205	2.84092	193.068	-40.314	2.105
Li^6	6.01458	1.89032	128.466	-26.824	1.400
Li^7	7.01546	1.62063	110.138	-22.998	1.201
N^{14}	14.00252	0.81197	55.181	-7.733	0.601
O^{16}	15.99436	0.71085	48.309	-6.770	0.527
H_2O	18.01002	0.63129	42.902	-6.016	0.468
N_2	28.00559	0.40640	27.590	-3.866	0.301
O_2	31.98927	0.35542	25.154	-3.385	0.263
CO_2	43.98927	0.25846	17.565	-2.461	0.191

Initial Distribution List

		No. Copies
1.	Defense Documentation Center Cameron Station Alexandria, Virginia 22314	20
2.	Library Naval Postgraduate School Monterey, California 93940	2
3.	Commander Naval Ordnance Systems Command Hq Washington, D.C. 20360	1
4.	Prof. Otto Heinz Department of Physics Naval Postgraduate School Monterey, California 93940	3
5.	Prof. R.L. Kelly Department of Physics Naval Postgraduate School Monterey, California 93940	1
6.	Dr. Charles Cook Stanford Research Institute (A220) Menlo Park, California	1
7.	Mr. Thomas Maris Department of Physics Naval Postgraduate School Monterey, California 93940	1
8.	Capt. W.B. Muncie, USN Commanding Officer, VX-5 Naval Air Facility China Lake, California	1
9.	Lt. Thomas O. Bush, USN Department of Physics Naval Postgraduate School Monterey, California 93940	1
10.	Lt. George H. Strohsahl, Jr. VA-42 NAS Oceana Virginia Beach, Virginia 23460	2

DOCUMENT CONTROL DATA - R&D

(Security classification of title, body of abstract and indexing annotation must be entered when the overall report is classified)

1. ORIGINATING ACTIVITY *(Corporate author)* Naval Postgraduate School Monterey, California 93940	2a. REPORT SECURITY CLASSIFICATION UNCLASSIFIED 2b. GROUP

3. REPORT TITLE
Construction and Calibration of a Mass Spectrometer for the Analysis of Light Ions

4. DESCRIPTIVE NOTES *(Type of report and inclusive dates)*
Thesis, MS, December 1967

5. AUTHOR(S) *(Last name, first name, initial)*
Strohsahl, George H., Jr., LT, USN

6. REPORT DATE	7a. TOTAL NO. OF PAGES	7b. NO. OF REFS
December 1967	65	13

8a. CONTRACT OR GRANT NO.	9a. ORIGINATOR'S REPORT NUMBER(S)
b. PROJECT NO.	
c.	9b. OTHER REPORT NO(S) *(Any other numbers that may be assigned this report)*
d.	

10. AVAILABILITY/LIMITATION NOTICES
[redacted]

11. SUPPLEMENTARY NOTES	12. SPONSORING MILITARY ACTIVITY

13. ABSTRACT A magnetic mass spectrometer employing a 45° bending angle was constructed and calibrated as part of an experimental apparatus to study ion-molecule rearrangement collisions. It has a resolution ($m/\Delta m$) of about 40 with beam transmission in excess of 90%, and it will mass analyze charged particles up to mass number 40 with energies up to 1 KEV. The spectrometer, using a magnet current of 8 amps, has a maximum field strength of about 4 Kilogauss confined between 40° wedge sector shaped pole pieces with a 3/4" gap width. Magnet current curves are given for mass analysis of ions through mass number 7 as a function of kinetic energy. A plasma source using electron-impact ionization was used to generate the ion beams of mass 1 to 4 while a thermal β-eucryptite source was used to produce Li^{+} beams of mass 6 and 7. Measurements of the energy spread of the ion beams indicate a typical value of $\Delta E/E = 4\%$ for the gas source and 1% for the thermal emitter. Subject to a specified degaussing procedure the beam energy can be written as a function of magnet current in the form $E = C_3 I^2 + C_2 I + C_1$. Tables giving both experimentally and theoretically determined values of the coefficients C_3, C_2 and C_1 as a function of ion mass are presented.

14. KEY WORDS	LINK A		LINK B		LINK C	
	ROLE	WT	ROLE	WT	ROLE	WT
Mass Spectrometer						
Mass Analysis						
Ion-Molecule Rearrangement Collisions						
Thermal Ion Source						
Electron Impact Ion Source						
Energy Analyzer						
Retarding Field						

[redacted]

thesS853
DUDLEY KNOX LIBRARY
3 2768 00414847 8
3 2768 002 02134 7
DUDLEY KNOX LIBRARY